iScience

CellPress
OPEN ACCESS

Article

TERC promotes non-small cell lung cancer progression by facilitating the nuclear localization of TERT

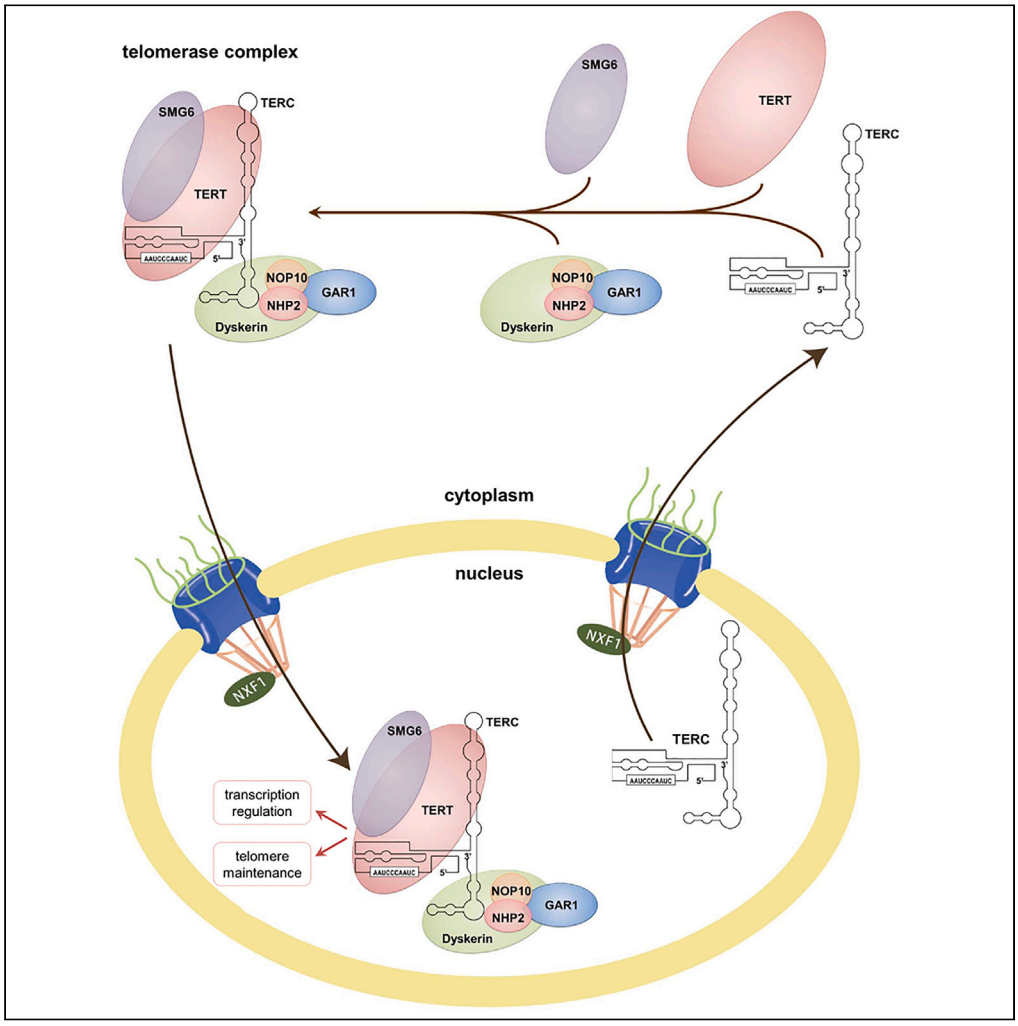

Haohui Sun, Xiaodi Li, Qian Long, ..., Chuyang Huang, Wuguo Deng, Miao Chen

dengwg@sysucc.org.cn (W.D.)
chenmiao@sysucc.org.cn (M.C.)

Highlights

Elevated TERC level is associated with NSCLC progression and unfavorable prognosis

TERC mediates the contact of TERT with other telomerase subunits in the cytoplasm

TERC depletion hinders the assembly and nuclear import of the telomerase complex

TERC facilitates the nuclear functions of TERT to promote NSCLC progression

Sun et al., iScience *27*, 109869
June 21, 2024 © 2024 The Authors. Published by Elsevier Inc.
https://doi.org/10.1016/j.isci.2024.109869

iScience

CellPress
OPEN ACCESS

Article

TERC promotes non-small cell lung cancer progression by facilitating the nuclear localization of TERT

Haohui Sun,[1,4] Xiaodi Li,[1,4] Qian Long,[1,2,4] Xiaonan Wang,[1] Wancui Zhu,[1] Enni Chen,[1] Wenhao Zhou,[1] Han Yang,[1] Chuyang Huang,[3] Wuguo Deng,[1,*] and Miao Chen[1,5,*]

SUMMARY

The core of telomerase consists of the protein subunit telomerase reverse transcriptase (TERT) and the telomerase RNA component (TERC). So far, the role of TERC in cancer development has remained elusive. Here, we found TERC expression elevated in non-small cell lung cancer (NSCLC) tissues, which was associated with disease progression and poor prognosis in patients. Using NSCLC cell lines and xenograft models, we showed that knockdown of TERC caused cell cycle arrest, and inhibition of cell proliferation and migration. Mechanistically, TERC was exported to the cytoplasm by nuclear RNA export factor 1 (NXF1), where it mediated the interaction of TERT with other telomerase subunits. Depletion of TERC hindered the assembly and subsequent nuclear localization of the telomerase complex, preventing TERT from functioning in telomere maintenance and transcription regulation. Our findings suggest that TERC is a potential biomarker for NSCLC diagnosis and prognosis and can be a target for NSCLC treatment.

INTRODUCTION

Non-small cell lung cancer (NSCLC) accounts for over 80% of the cases in lung cancer, which is the leading cause of cancer-related deaths globally.[1] Despite recent advances in surgical procedures, novel therapies, and effective clinical management, the overall survival of patients with NSCLC remains poor.[2] Therefore, it is of importance to further improve treatment strategies for NSCLC.

Telomerase is a ribonucleoprotein complex with reverse transcriptase activity, which counteracts telomere shortening during cell division by adding the 5′-TTAGGG-3′ DNA repeat to the ends of chromosomes to maintain telomere length.[3,4] The two essential components of the telomerase complex are the catalytic protein subunit telomerase reverse transcriptase (TERT) and the telomerase RNA component (TERC), which serves as the template for telomere DNA synthesis.[5,6] The expression of TERT is suppressed in human somatic cells[7,8] but dramatically elevated in over 85% of malignant tumors, which is the prerequisite for telomerase activation and cell immortalization.[9–11] Accordingly, TERT has been deemed a promising cancer-specific target, and a variety of telomerase inhibitors have been developed. For example, BIBR1532 is a selective small-molecule compound that non-competitively targets TERT, leading to progressive telomere shortening in cancer cells, but its poor pharmacokinetic properties have limited its clinical applicability.[12,13] Alternatively, the oligonucleotide-based compound imetelstat prevents template annealing of TERC with the 3′ single-stranded telomeric overhang, and it has entered clinical trials. Nevertheless, in a phase 2 trial on NSCLC patients, only patients with short telomeres tended to have improved progression-free survival and overall survival after imetelstat treatment,[14] which could be due to the delay needed for the anti-tumor effects resulting from critical telomere shortening.[13]

Importantly, the functions of TERT are not limited to telomere maintenance. Accumulating evidence suggests that TERT can promote cancer formation by means independent of telomere.[15–17] For instance, TERT was shown to stimulate the transcription of targets of the Wnt/β-catenin pathway, such as c-Myc and cyclin D1.[18] Also, TERT was found to bind at the promoter of the vascular epithelial growth factor (VEGF) gene and promote angiogenesis.[19] Furthermore, TERT was reported to associate with ribosomal RNA (rRNA) and transfer RNA (tRNA) genes to promote their transcription.[20,21] In addition, TERT is present in mitochondria, where it protects mitochondrial DNA from oxidative stress, increases respiratory chain activity, and lowers cellular reactive oxygen species (ROS) level.[22,23] Currently, it is unclear whether TERT inhibitors like BIBR1532 affect the telomere-independent activities of TERT.

Unlike TERT, the long non-coding RNA (lncRNA) component TERC is ubiquitously expressed in human cells and tissues regardless of their telomerase activity.[24,25] Nevertheless, studies have indicated that TERC also plays important roles in cancer and other proliferating cells.

[1]State Key Laboratory of Oncology in South China and Collaborative Innovation Center for Cancer Medicine, Sun Yat-sen University Cancer Center, Guangzhou, Guangdong 510060, China
[2]Department of General Surgery, The Second Xiangya Hospital, Central South University, Changsha, Hunan 410011, China
[3]Department of Urology, Shaoyang Central Hospital, University of South China, Shaoyang, Hunan 422000, China
[4]These authors contributed equally
[5]Lead contact
*Correspondence: dengwg@sysucc.org.cn (W.D.), chenmiao@sysucc.org.cn (M.C.)
https://doi.org/10.1016/j.isci.2024.109869

This is an open access article under the CC BY-NC-ND license (http://creativecommons.org/licenses/by-nc-nd/4.0/).

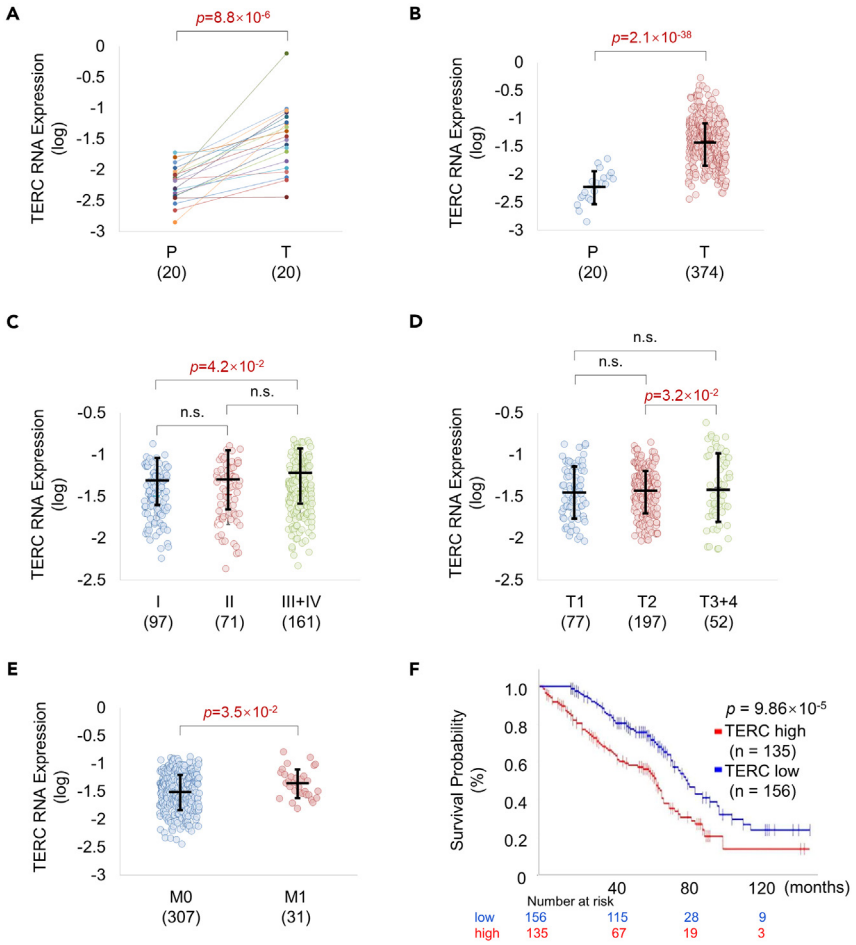

Figure 1. Elevated TERC level in NSCLC tissues is correlated with disease progression and shorter overall survival

(A) RNA levels of TERC in 20 pairs of para-tumor (P) and tumor (T) tissues.

(B) RNA levels of TERC in 20 para-tumor (P) and 374 tumor (T) tissues.

(C–E) Dot distribution graphs of TERC RNA levels in NSCLC tissues of different stage (C), T category (D), and distant metastasis (E).

(F) Kaplan-Meier's survival analysis of NSCLC patients with high and low TERC expression. The best cutoff value of TERC level was determined by the X-tile software. RNA was extracted from tissue samples in the SYSUCC cohort, and RT-qPCR was performed to measure the relative levels of TERC, using β-actin as an internal control. The numbers of patients in each group were indicated in the brackets. *p* values in (A–E) were determined by Student's *t*-test, n.s. stands for non-significant statistically; data in (B–E) were also presented as mean ± SD; *p* value in (F) was calculated by the log rank test.

TERC is not only necessary for the tumor-promoting effects of TERT overexpression,[26] but its up-regulation is also an early event in tumorigenesis, while telomerase activity is detected in the late stages of tumor progression.[27] In immune cells, knockdown of TERC induced apoptosis without triggering telomere shortening or DNA damage response,[28] and TERC was found to promote $CD4^+$ T cell proliferation by activating AKT independently of telomerase activity.[29]

In NSCLC, expression of TERC was elevated in tumor tissues compared to their non-tumorous counterparts,[30] but its regulatory mechanism and clinical relevance remain unclear. In this study, we investigated the expression of TERC, its regulation, clinical significance, and cellular roles in NSCLC. Additionally, we explored whether TERC could be a therapeutic target in NSCLC.

RESULTS

Elevated expression of TERC is associated with NSCLC development and progression

To explore the clinical significance of the lncRNA TERC, we first examined TERC expression in our Sun Yat-sen University Cancer Center (SYSUCC) cohort, which had 20 pairs of NSCLC and adjacent tissue samples and another 354 tumor tissue samples. Pairwise analysis showed that TERC lncRNA level was significantly elevated in all (20/20) tumor samples (Figure 1A), while only half (10/20) of the tumors had higher TERT mRNA level when compared to the matching para-tumor tissues (Figure S1A). Overall, the RNA level of TERC was remarkably higher in tumor tissues (Figure 1B), which was not observed in the analysis of TERT mRNA in NSCLC and para-tumor tissue samples (Figure S1B). Our finding

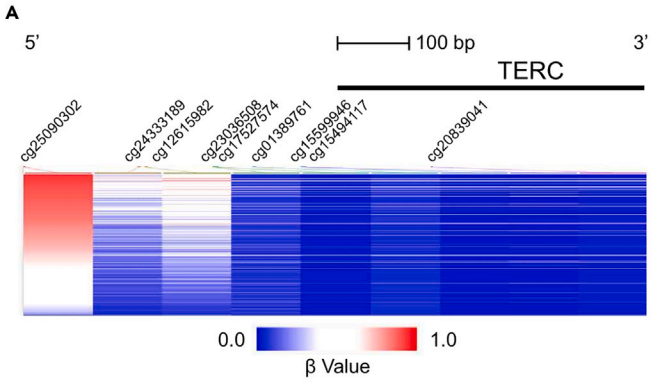

C

Correlation of TERC promoter methylation with RNA expression

	Spearman's ρ	*p*-value
cg25090302	-0.211	6.8×10^{-4}
cg24333189	-0.186	2.3×10^{-3}
cg12615982	-0.172	5.5×10^{-3}

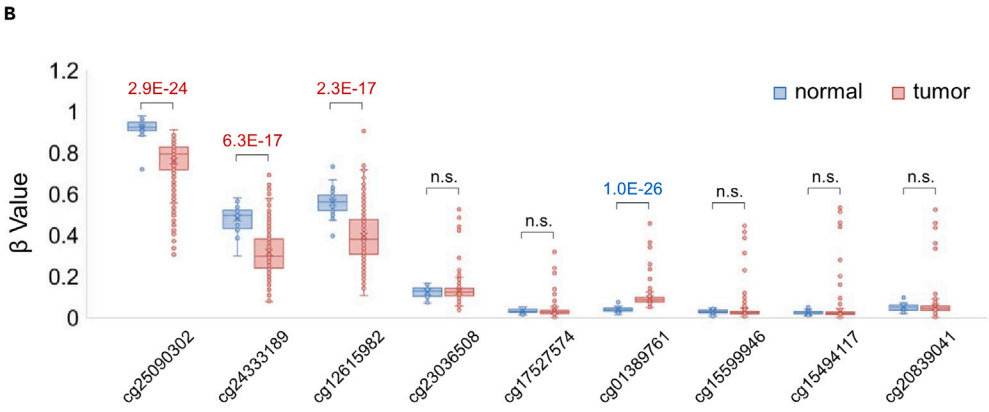

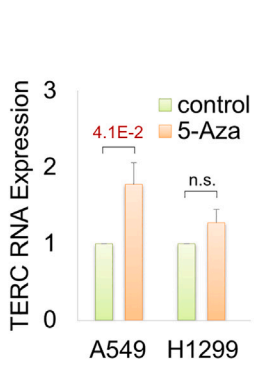

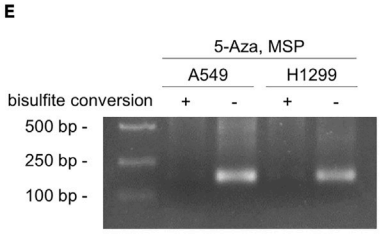

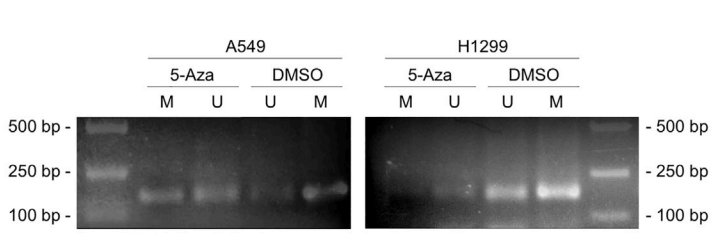

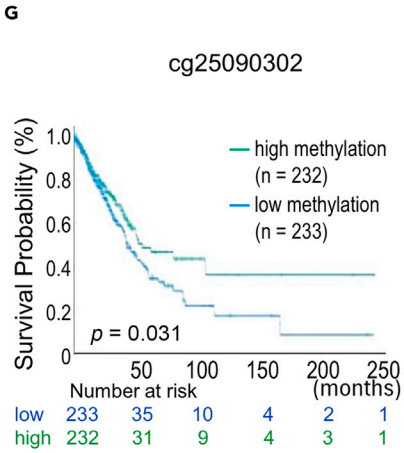

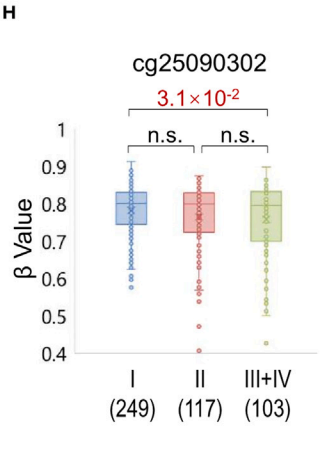

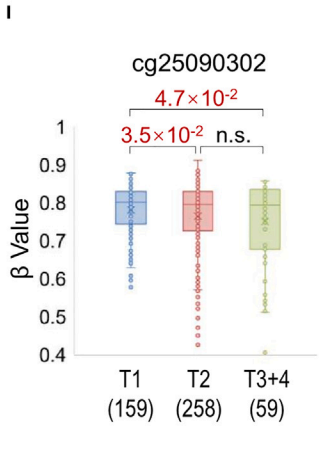

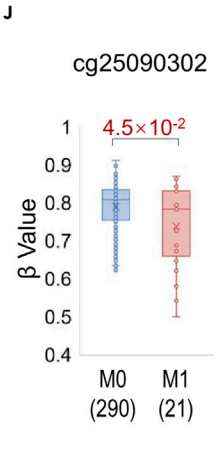

Figure 2. TERC promoter methylation is altered in NSCLC tissues

(A) DNA methylation level (β value) of CpG sites in the promoter region and gene body of TERC in NSCLC patients. The modified illustration was exported from UCSC Xena (https://xena.ucsc.edu/), and genomic data of the TCGA-NSCLC cohort were explored.

Figure 2. *Continued*

(B) Box and whisker plot of DNA methylation level of the 9 CpG sites (cg25090302, cg24333189, cg12615982, cg23036508, cg17527574, cg01389761, cg15599946, cg15494117, and cg20839041) located in TERC promoter and gene body in NSCLC (n = 503) and normal lung (n = 32) tissues.

(C) Correlation of TERC promoter methylation with RNA expression.

(D) Relative RNA level of TERC in NSCLC cells treated with or without 5-azacytidine (5-Aza). RNA extracts were prepared from A549 and H1299 cells treated with 5 μM 5-Aza or DMSO (as control) for 48 h, and RT-qPCR was performed. Data were presented as mean ± SD (n = 3).

(E) Validation of the efficiency of 5-Aza treatment and bisulfite conversion. Genomic DNA was extracted from 5-Aza-treated A549 and H1299 cells and further treated with (+) or without (−) sodium bisulfite, which converted the unmethylated cytosines of the genomic DNA to uracils, but not the methylated cytosines. A region of 165 bp in the TERC promoter was amplified with the methylation-specific PCR (MSP) primer set designed by MethPrimer.[32]

(F) Representative images of MSP products. DNA was prepared from A549 and H1299 cells treated with 5-Aza or DMSO. After bisulfite conversion, a 165 bp region in the TERC promoter was amplified by one primer pair specific for a methylated state (M) and the other pair for an unmethylated state (U).

(G) Kaplan-Meier's survival analysis of NSCLC patients with high and low methylation in the cg25090302 locus. p value was calculated by the log rank test.

(H–J) Box and whisker plots of cg25090302 methylation levels in NSCLC tissues of different stage (H), T category (I), and distant metastasis (J). p values in (B, D, H–J) were determined by Student's t-test, n.s. stands for non-significant statistically; p value in (G) was calculated by the log rank test.

from the SYSUCC cohort was verified in the public dataset GEO: GSE32863,[31] which showed that TERC lncRNA level was higher in tumors in 26 out of 45 pairs of samples, but TERT mRNA level was higher in tumors in fewer than half (20/45) of the paired samples (Figure S2A).

In order to clarify the clinical correlation between TERC expression and NSCLC progression, we further analyzed the data of our SYSUCC cohort. We found increased TERC lncRNA level was preferentially correlated with cancer stage (I vs. III/IV, p = 0.0420; Figure 1C), T category (T1 vs. T3+4, p = 0.0506; T2 vs. T3+4, p = 0.0323; Figure 1D), and distant metastasis (M0 vs. M1, p = 0.0346; Figure 1E). Kaplan-Meier's survival analysis indicated that higher TERC level was strongly associated with shorter overall survival ($p = 9.86 \times 10^{-5}$; Figure 1F). By contrast, TERT mRNA level in NSCLC tissues indicated no obvious association with disease progression or prognosis in patients (Figures S1C–S1F). Consistent with the results from our SYSUCC cohort, analysis of The Cancer Genome Atlas (TCGA) cohort confirmed that elevated TERC lncRNA level was significantly correlated with advanced cancer stage (I vs. III/IV, p = 0.0206; II vs. III/IV, p = 0.0277; Figure S2B), and shorter overall survival of NSCLC patients (p = 0.0245; Figure S2D), though such correlations were not statistically significant in terms of T category (T1 vs. T3+4, p = 0.171; Figure S2C). Also, TERT mRNA level was not significantly associated with disease stage, T category, or patients' survival (Figures S2B–S2D). Collectively, our findings suggest that TERC expression is frequently up-regulated in primary NSCLC, which is associated with disease progression and unfavorable prognosis.

TERC promoter methylation is correlated with TERC expression in NSCLC

We then sought to elucidate the mechanism that regulates the expression of TERC in NSCLC. As DNA methylation alters the accessibility of genes to transcription factors, it plays an important role in epigenetic gene regulation. We analyzed DNA methylation data from the HumanMethylation450 BeadChip in the TCGA cohort, using probes cg25090302, cg24333189, cg12615982, cg23036508, cg17527574, cg01389761, cg15599946, cg15494117, and cg20839041 that target CpG sites in the promoter region and gene body of TERC (Figure 2A). Our result showed that cg25090302, cg24333189, and cg12615982 in the TERC promoter region were noticeably hypermethylated under normal condition, but their methylation level was dramatically decreased in NSCLC tissues (Figure 2B). Moreover, DNA methylation of these three CpG sites was in significant negative correlation with TERC RNA level (Figures 2C and S3A), indicating that hypomethylation of TERC promoter contributed to increased expression of TERC in NSCLC. To confirm this, we treated A549 and H1299 cells with DNA methylation inhibitor 5-azacytidine (5-Aza). Methylation-specific PCR showed that the TERC promoter became less methylated after 5-Aza treatment (Figures 2E and 2F), and quantitative reverse-transcription PCR (RT-qPCR) proved that TERC expression was increased (Figure 2D). We also compared the methylation level of the TERC promoter in paired NSCLC and adjacent tissues. We observed a trend of decrease in TERC promoter methylation in tumor tissues, though it was not statistically significant due to the small sample size (Figure S3B).

Next, we investigated whether TERC promoter methylation could be a prognostic factor in NSCLC. We found that higher methylation of cg25090302, cg24333189, and cg12615982 was associated with longer overall survival (Figures 2G and S3C). In addition, the methylation level of cg25090302 was negatively correlated with cancer stage (I vs. III/IV, p = 0.0315; Figure 2H), T category (T1 vs. T2, p = 0.0345; T1 vs. T3+4, p = 0.0469; Figure 2I), and distant metastasis (M0 vs. M1, p = 0.0453; Figure 2J).

Alteration in DNA copy number can also lead to deregulation of RNA expression. Our analysis of both the SYSUCC and the TCGA cohorts showed a positive correlation between TERC gene copy number and RNA level, but no clear association was found between TERC DNA abundance and overall survival in NSCLC patients (Figure S4). Our aforementioned data imply that hypomethylation of TERC promoter is a major cause of the increased expression of TERC in NSCLC, which may serve as an indicator for disease development and poor prognosis.

Knockdown of TERC inhibits NSCLC cell growth

To confirm the cellular role of TERC, we knocked down TERC in NSCLC cell lines A549, H322, H460, and H1299, using TERC-specific siRNAs that had no impact on TERT mRNA expression (Figures 3A and S5A). Colony formation assay showed that proliferation of NSCLC cells with TERC down-regulated was notably inhibited (Figure 3B). Also, silencing of TERC led to decreased migration capacity and cell cycle arrest in G1 phase in NSCLC cells (Figures 3C and 3D).

Subsequently, we established A549 and Lewis lung carcinoma cells with TERC stably knocked down. In concordance with the *in vitro* results, stable silencing of TERC significantly reduced xenograft tumor burden (Figures 4A and 4B). Immunohistochemistry staining of A549

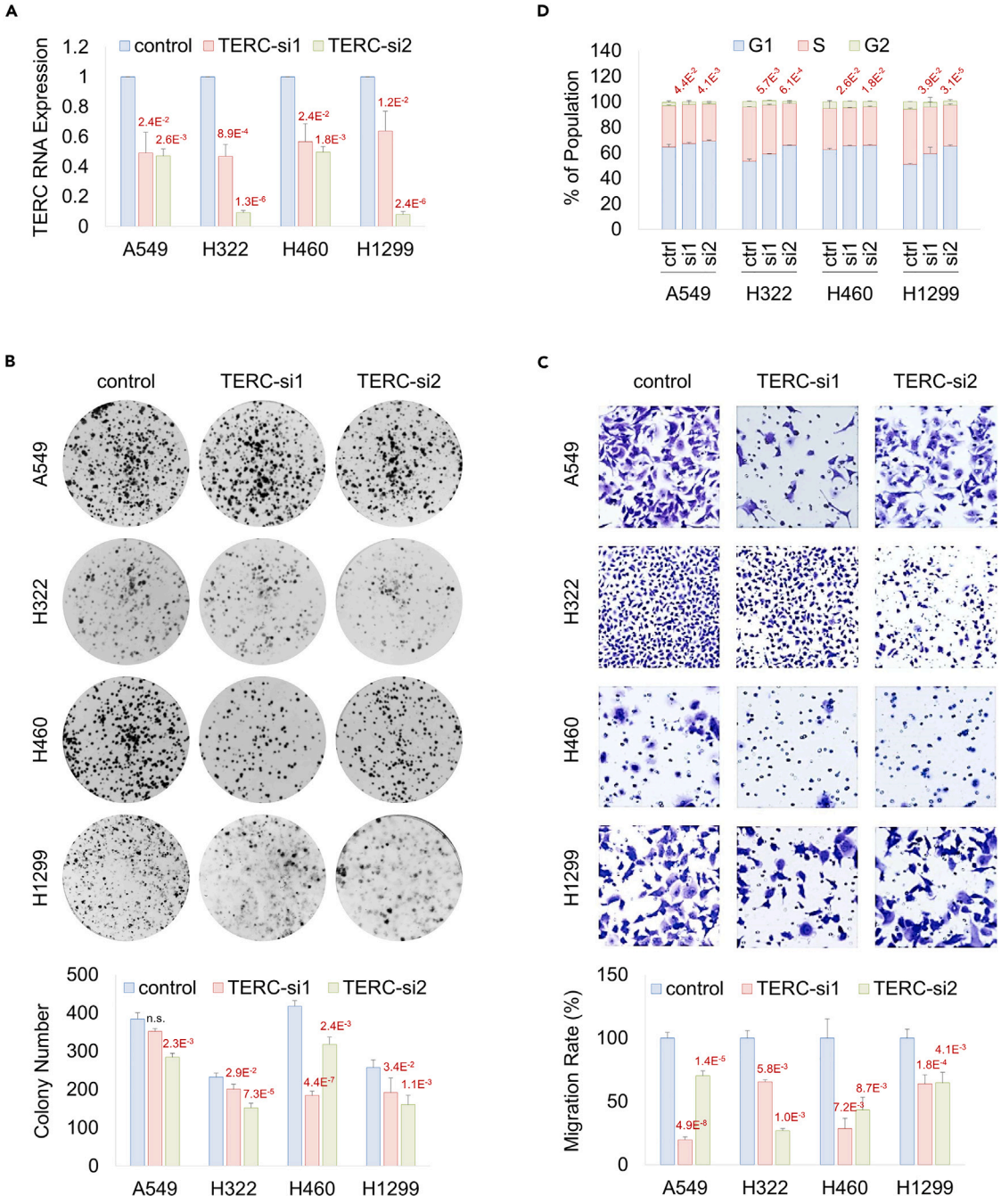

Figure 3. Down-regulation of TERC inhibits NSCLC cell proliferation and migration *in vitro*

(A) Relative RNA level of TERC in NSCLC cells. Whole-cell RNA extracts were prepared from A549, H322, H460, and H1299 cells without (control) or with TERC knockdown (TERC-si1, TERC-si2), and RT-qPCR was performed for each extract, using U6 small nuclear RNA as an internal control.

(B) Cell proliferation capacity evaluated by colony formation assay. Representative images were shown on the top panel. Quantification was presented on the bottom panel.

(C) Cell migration ability determined by transwell assay. Representative images were shown on the top panel, and relative migration rates were presented on the bottom panel.

(D) Cell cycle progression analyzed by fluorescence-activated cell sorting (FACS) assay. A549, H322, H460, and H1299 cells were transfected with control (ctrl) or TERC-specific siRNAs (si1 and si2), fixed with 70% ethanol and stained with propidium iodide (PI) before analyzed by FACS. Each trial included at least 10,000 cells. Data in all panels were presented as mean ± SD ($n \geq 3$), and p values between the control and the TERC-si1/2 groups were calculated by Student's t-test, n.s. stands for non-significant statistically.

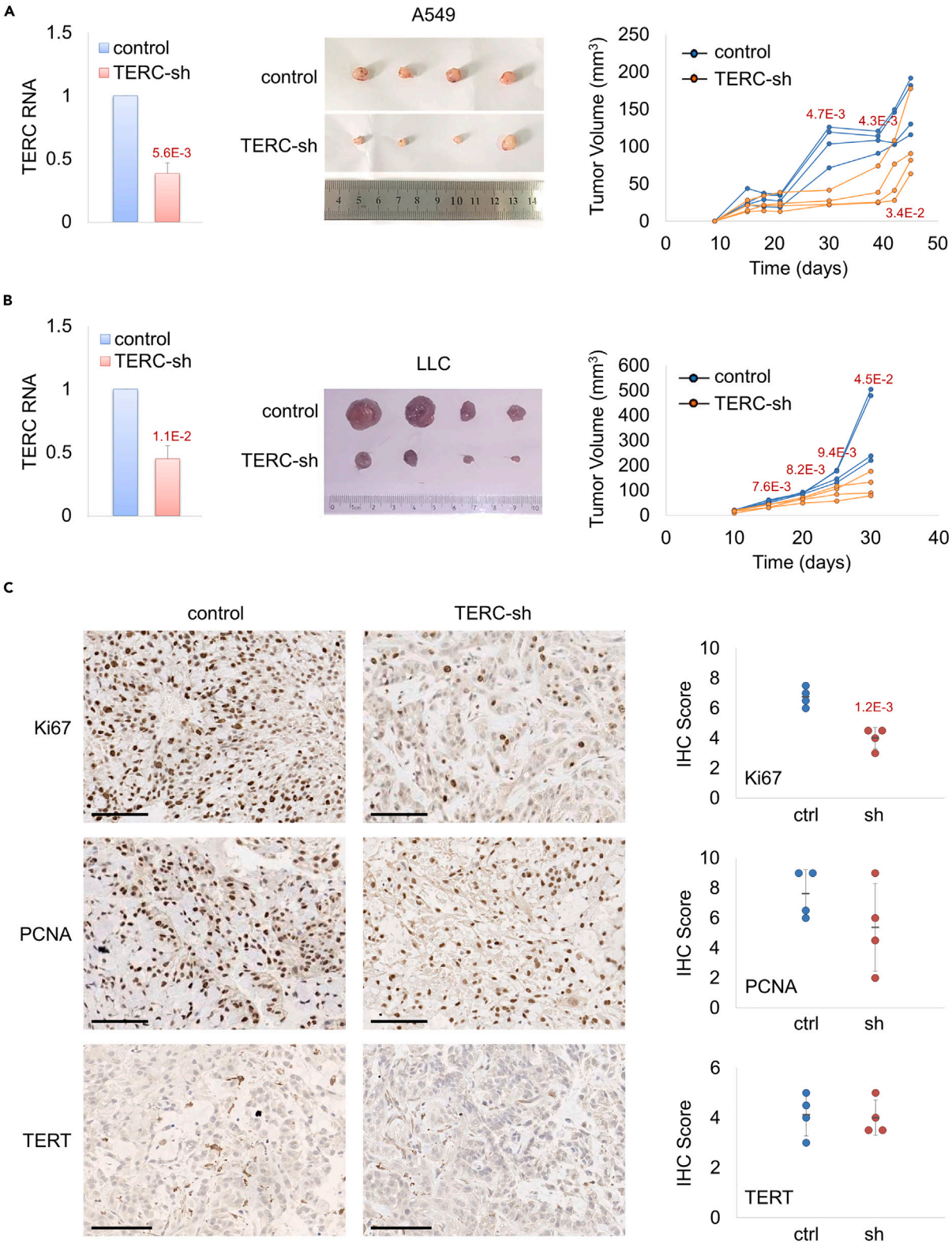

Figure 4. Knockdown of TERC suppresses NSCLC growth *in vivo*

(A and B) Left: Relative RNA level of TERC in A549 (A) and Lewis lung carcinoma (LLC) (B) cells without (control) or with TERC stably knocked down (TERC-sh). Middle: Xenograft tumors from A549 and LLC cells. Right: Growth of xenograft tumors over time.

Figure 4. *Continued*

(C) Left: Representative images (20× magnification) of immunohistochemistry (IHC) staining to detect Ki67, PCNA, and TERT levels in xenograft tumors from A549 cells. Scale bar, 100 μm. Right: Quantification of IHC scores in xenograft tumors without (ctrl) or with TERC stably knocked down by shRNA (sh). Data were presented as mean ± SD (n = 4), and p values were determined by Student's t-test.

xenograft tumor sections showed inhibited proliferation indicated by Ki67 and PCNA staining in TERC-depleted cells (Figure 4C). These results implicate that TERC promotes NSCLC cell growth and proliferation.

Knockdown of TERC suppresses the nuclear functions of TERT

Considering that TERC is one of the two essential components of telomerase, we tested whether it played the oncogenic role in NSCLC through its interaction partner TERT. We first assessed the telomere length in NSCLC cells. As shown in Figure 5A, knockdown of TERC remarkably shortened the relative telomere length, which was comparable to the effect of BIBR1532, the telomerase inhibitor that causes progressive telomere shortening without affecting the expression of TERT (Figure S5B). Furthermore, we examined whether TERT stimulated the expression of rRNAs, tRNAs, and Wnt target genes in a TERC-dependent manner in A549 cells. Chromatin immunoprecipitation (ChIP) qPCR revealed that TERT bound to the promoter regions of tRNA-Arg, tRNA-Leu, tRNA-Lys, tRNA-Met, c-Myc, cyclin D1, and VEGF, but not the rRNA genes, and such binding was lost in the absence of TERC (Figure 5B). Consistently, RT-qPCR confirmed that knockdown of TERC reduced the transcripts of the nascent pre-tRNAs and the Wnt target genes tested (Figure 5C). Noteworthily, inactivation of TERT with BIBR1532 in A549 cells neither abolished the association of TERT with its target genes, nor impeded their transcription (Figures 5B and 5C), indicating that the enzymatic activity of TERT is nonessential to its functions in chromatin binding and transcription regulation.

The *in vitro* results described above were further supported by data from A549 xenograft tumor RNA extracts (Figure 5D). Also, gene expression correlation analysis of the NSCLC patient samples in the GEO: GSE32863 dataset revealed that the TERC RNA level was positively correlated with the mRNA levels of c-Myc, Cyclin D1 and VEGF (Figure S6A). Likewise, TERT mRNA expression was positively correlated with those of c-Myc, Cyclin D1 and VEGF (Figure S6B). Moreover, in the TCGA cohort, DNA methylation of the TERC promoter was negatively correlated with the mRNA expression of c-Myc, cyclin D1, and VEGF (Figure S6C). Nonetheless, no correlation was found between TERC gene copy number and c-Myc, cyclin D1, and VEGF mRNA levels (Figure S6D). In addition, western blotting showed that the protein level of cyclin D1 was lowered in the absence of TERC (Figure 5E), which was in consistence with G1 phase cell cycle arrest (Figure 3D). These data suggest that increased expression of TERC due to promoter hypomethylation enhances the functions of TERT in the nucleus of NSCLC cells.

We also tested the mitochondrial functions of NSCLC cells with TERC absent, as studies have shown that cytoplasmic TERT can be localized to mitochondria to protect cells from oxidative stress.[34] Our results showed that knockdown of TERC had negligible effects on intracellular ROS and mitochondrial membrane potential (Figures S7A and S7B). Similarly, inhibition of TERT activity by BIBR1532 did not alter the ROS level in NSCLC cells (Figure S7C). These observations implicate that neither TERC nor TERT activity is indispensable to the mitochondrial functions of NSCLC cells under non-stress conditions.

TERC promotes the nuclear localization of TERT

To understand how TERC promotes the nuclear functions of TERT in NSCLC cells, we investigated if TERC mediated the nuclear localization of TERT by nucleocytoplasmic fraction experiments. We found that knockdown of TERC had no obvious effect on the total protein amount of TERT in NSCLC cells, whereas the nuclear level of TERT decreased dramatically (Figures 6A and S8). Consistently, immunofluorescence assay showed that TERT was predominantly nuclear in control cells, whereas it was evenly distributed between the nucleus and the cytoplasm when TERC was depleted (Figure 6B). Moreover, immunohistochemistry staining of xenograft tumor sections demonstrated that TERT staining was more prevalent in the cytoplasm of cells with TERC stably knocked down, compared to cells of the control group (Figure 6C).

In budding yeast, TLC1 (the ortholog of human TERC) was found to mediate the assembly of the telomerase complex in the cytoplasm.[35] In concordance with this, our co-immunoprecipitation experiment demonstrated that the interaction between TERT and SMG6 (also known as EST1A, a subunit of the telomerase) decreased when the level of TERC was reduced in NSCLC cells (Figure 7A). Noteworthily, down-regulation of TERC also prevented the nuclear localization of SMG6 without affecting its total amount (Figure 7B). We hence speculated that TERT need to associate with cytoplasmic TERC and other telomerase components to form the ribonucleoprotein complex before entering the nucleus, and impaired nucleo-cytoplasmic shuttling of TERC might impact the nuclear localization of TERT. A recent study reported that nuclear RNA export factor 1 (NXF1) preferentially mediated the nuclear export of lncRNAs and mRNAs with few exons.[36] Our RNA immunoprecipitation assay confirmed that NXF1 interacted with TERC in A549 cells while exportin 1 (XPO1) did not (Figure 8A), though it was implicated in the nuclear export of the TLC1 RNA in yeast.[35] We then knocked down NXF1 and measured the total amount and the nuclear fraction of TERC, respectively. RT-qPCR data proved that TERC was retained in the nucleus in the absence of NXF1, despite its unaltered level in whole cells (Figures 8B and S9A), proving that NXF1 mediated the nuclear export of TERC. Importantly, western blotting revealed decreased nuclear level of TERT in A549 cells with NXF1 knockdown (Figures 8C and 8D). Consistently, the relative telomere length was shortened in NSCLC cells with NXF1 silenced (Figure 8E), while the mitochondrial functions remained unaffected (Figure S9B). These results support the notion that TERC is a limiting factor for the cytoplasmic assembly of the telomerase and its subsequent translocation to the nucleus.

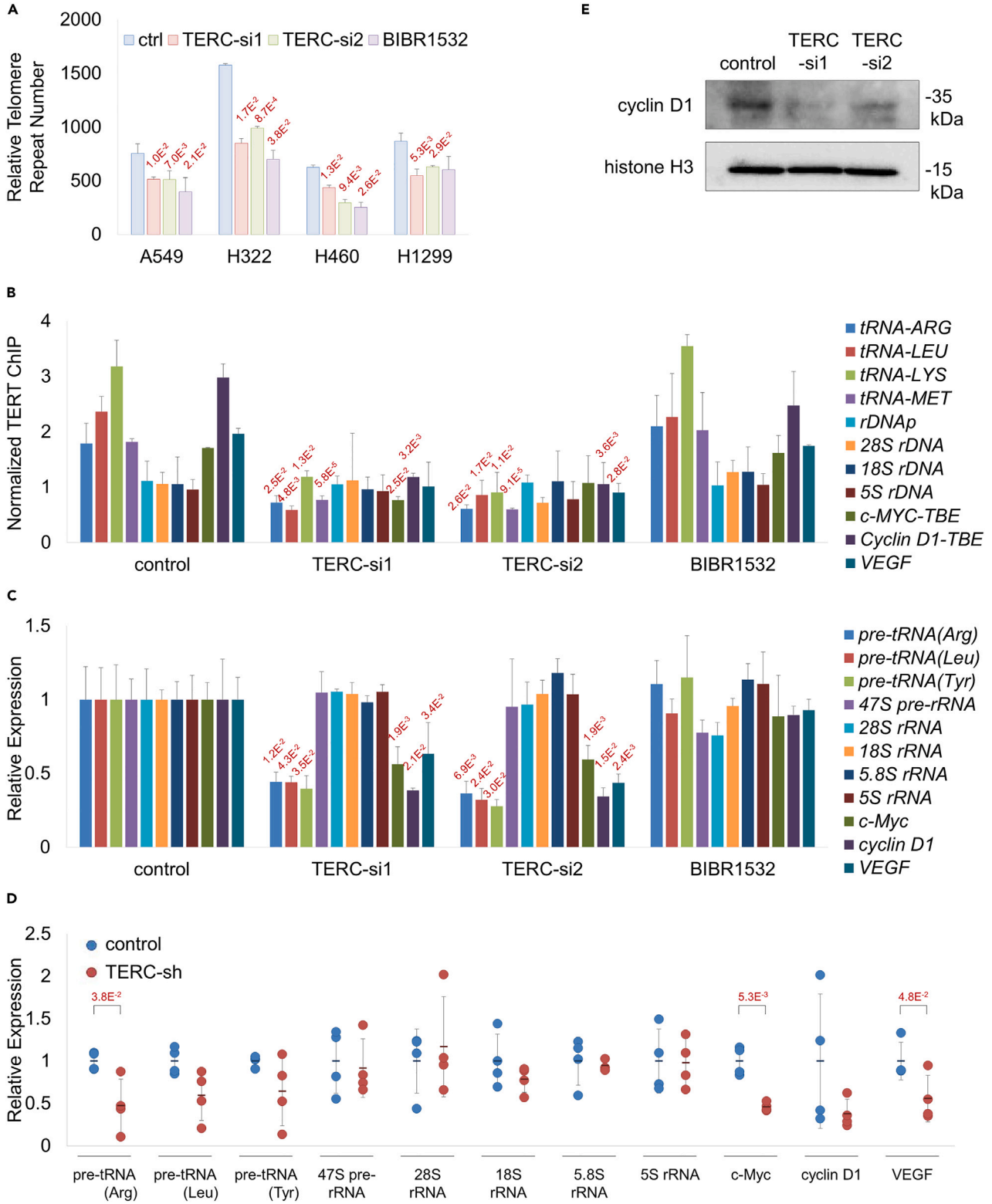
A
Relative Telomere Repeat Number
2000
1500
1000
500
0
ctrl
TERC-si1
TERC-si2
BIBR1532
1.0E-2
7.0E-3
2.1E-2
1.7E-2
8.7E-4
3.8E-2
1.3E-2
9.4E-3
2.6E-2
5.3E-3
2.9E-2
A549
H322
H460
H1299
E
control
TERC -si1
TERC -si2
cyclin D1
-35 kDa
histone H3
-15 kDa
B
Normalized TERT ChIP
4
3
2
1
0
control
TERC-si1
TERC-si2
BIBR1532
tRNA-ARG
tRNA-LEU
tRNA-LYS
tRNA-MET
rDNAp
28S rDNA
18S rDNA
5S rDNA
c-MYC-TBE
Cyclin D1-TBE
VEGF
C
Relative Expression
1.5
1
0.5
0
control
TERC-si1
TERC-si2
BIBR1532
pre-tRNA(Arg)
pre-tRNA(Leu)
pre-tRNA(Tyr)
47S pre-rRNA
28S rRNA
18S rRNA
5.8S rRNA
5S rRNA
c-Myc
cyclin D1
VEGF
D
Relative Expression
2.5
2
1.5
1
0.5
0
control
TERC-sh
3.8E-2
5.3E-3
4.8E-2
pre-tRNA (Arg)
pre-tRNA (Leu)
pre-tRNA (Tyr)
47S pre-rRNA
28S rRNA
18S rRNA
5.8S rRNA
5S rRNA
c-Myc
cyclin D1
VEGF

Figure 5. Knockdown of TERC inhibits the nuclear functions of TERT

(A) Relative telomere repeat number in NSCLC cells. Cellular DNA was extracted from A549, H322, H460, and H1299 cells without (ctrl) or with TERC knockdown (TERC-si1, TERC-si2), or treated with 10 μM BIBR1532, and qPCR was performed for each extract to obtain the relative telomere repeat number as described previously,[33] using 36B4 as the single-copy gene control.

(B) Binding of TERT at the indicated genomic regions. ChIP was performed with TERT antibody, or IgG as control, and qPCR was run with primers specific for the tested target regions in A549 cells without or with TERC knockdown, or treated with 10 μM BIBR1532. Reported values correspond to the signal for each site relative to that of the IgG control.

(C) Gene expression analysis of pre-tRNA, pre-rRNA, rRNA, as well as c-Myc, cyclin D1, and VEGF mRNA transcripts in A549 cells. RT-qPCR was performed, and U6 served as the control for pre-tRNA, pre-rRNA, and rRNA transcripts, while β-actin served as the control for mRNA transcripts. Data in (A–C) were presented as mean ± SD ($n \geq 2$), and p values between the control and the TERC-si1/2 groups were calculated by Student's t-test.

(D) Gene expression analysis in xenograft tumors from A549 cells without (control) or with TERC stably knocked down (TERC-sh). Data were presented as individual dots and mean ± SD ($n = 4$), and p values were determined by Student's t-test.

(E) Protein expression of cyclin D1. Western blotting was used to detect cyclin D1 levels in A549 cells. Histone H3 served as the loading control.

DISCUSSION

Clinical significance of TERC

Telomerase, the ribonucleoprotein complex that maintains the repetitive telomeric sequences at the ends of chromosomes, is largely absent in human normal somatic cells. However, telomerase is reactivated in the vast majority of cancer cells, contributing to telomere maintenance and replicative immortality.[10] The core components of telomerase are the catalytic protein subunit TERT and the lncRNA TERC as the template for telomere replication.[38] TERT has long been considered as the sole limiting factor for telomerase activity. For one thing, it is expressed only in telomerase-positive cells.[9,39] For another, expression of exogenous TERT alone is sufficient to immortalize normal human cells,[40] whereas inhibition of TERT leads to telomere shortening and apoptosis in cancer cells.[41,42]

In contrast to TERT, the expression of lncRNA TERC has been detected in various cells, including primary cells that have no telomerase activity.[25] Nevertheless, accumulating evidence suggests that TERC also plays an essential role in telomerase activity and cancer development. For example, overexpression of both TERC and TERT remarkably induced telomerase activity and telomere elongation in telomerase-positive cells, while overexpression of either TERC or TERT alone had a lesser effect.[43] Consistently, overexpression of TERT in the skin of TERC-deficient mice failed to promote tumorigenesis or wound healing.[26] These studies reinforce that both TERT and TERC are indispensable for a functional telomerase. Although TERC is expressed ubiquitously, its level is higher in germline and cancer cells than in normal somatic cells that have undetectable telomerase activity, and its down-regulation resulted in telomere shortening in HeLa cells.[44] In line with this, increased copy numbers of the TERC gene locus (at human chromosome band 3q26.3) have been detected in a few human cancers, such as cervical carcinoma, head and neck squamous cell carcinoma, and lung squamous cell carcinoma.[45,46]

To date, little is known about the regulation and the clinical significance of lncRNA TERC expression in NSCLC. In this study, we collected tissue samples from 374 NSCLC patients and used RT-qPCR to measure the abundance of different RNA species. We first found that TERC level was consistently higher in NSCLC tissues than in matched normal lung tissues (Figure 1A), and the increase of TERC expression in NSCLC tissues was far more significant than that of TERT (Figures 1B, S1, and S2). Next, we uncovered that elevated TERC expression was correlated with disease progression and shorter overall survival (Figures 1C–1F). We further explored the mechanism that regulates TERC expression in NSCLC. DNA methylation is closely associated with transcription regulation.[47] Our analysis of the DNA methylation status of the TERC gene and its flanking region revealed that the CpG sites cg25090302, cg24333189, and cg12615982 in the promoter of TERC were normally hypermethylated. However, the methylation level of these sites became significantly lower in NSCLC tissues, and it was negatively associated with TERC gene expression (Figures 2A–2C), which is concordant with the current model of epigenetic regulation whereby DNA methylation in this region often represses gene transcription.[47] Additionally, we observed that decreased methylation of cg25090302, cg24333189, and cg12615982 was associated with shorter overall survival (Figures 2G and S3C), and hypomethylation of cg25090302 was correlated with advanced cancer stage, T category, and distant metastasis (Figures 2H–2J). Of note, albeit we found that the gene copy number of TERC was positively correlated with its RNA level, TERC DNA abundance was insufficient to predict overall survival in NSCLC patients (Figure S4), suggesting that TERC promoter methylation might play a dominant role in the regulation of TERC expression. In conclusion, our findings indicate that DNA methylation and RNA expression of TERC may serve as a biomarkers for NSCLC diagnosis and prognosis.

Cellular functions of TERC

To understand the role of TERC in NSCLC cells, we knocked down its expression, which caused inhibition of cell proliferation, suppression of cell migration and cell cycle arrest (Figure 3), as well as retarded xenograft tumor growth in mice (Figure 4). We further investigated whether the growth inhibition in TERC-depleted NSCLC cells was related to TERT. Our results showed that the absence of TERC not only led to reduced telomere length, but also impaired the association of TERT with its target genes, which include a number of tRNA genes, c-Myc, cyclin D1, and VEGF, thus repressing their transcription (Figure 5). On the other hand, we saw little change in mitochondrial membrane potential and intracellular ROS level (Figure S7). Given that TERC knockdown mainly affected the nuclear functions of TERT, we assumed that TERC modulated the nuclear localization of TERT in NSCLC cells. In support of this notion, our experiment proved that the amount of TERT in the nucleus was noticeably reduced in TERC-depleted NSCLC cells (Figure 6).

Previously, TERT was reported to contain a nuclear localization signal (NLS) in amino acid residues 222–240.[48] However, mutations in this NLS had minimal effects on telomerase activity, suggesting there could be additional mechanisms regulating the nuclear-cytoplasmic

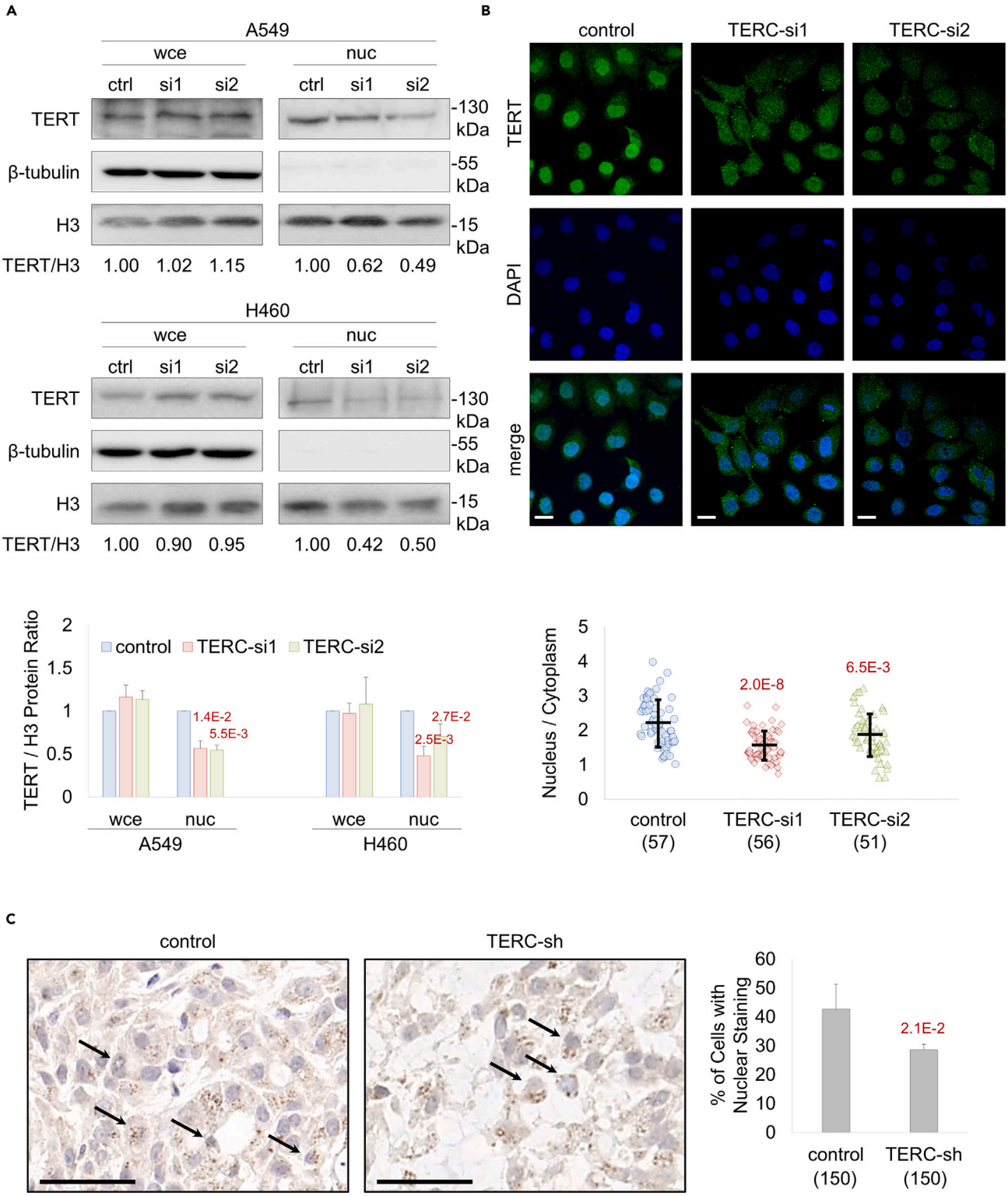

Figure 6. Knockdown of TERC blocks the nuclear localization of TERT

(A) Top and middle: Representative images of western blotting to detect the level of TERT in whole-cell extracts (wce) and nuclear extracts (nuc) of A549 and H460 cells without (ctrl) or with TERC knocked down (si1 and si2). β-tubulin served as whole cell and cytoplasmic loading control, while histone H3 served as whole cell and nuclear loading control. Numbers indicate the ratios of TERT/histone H3. Bottom: Quantification of the blots. Data were presented as mean ± SD ($n \geq 3$).

Figure 6. *Continued*

(B) Top: Representative images of the subcellular localization of TERT detected by immunofluorescence in A549 cells. Nuclei were stained with DAPI. Scale bar, 10 μm. Bottom: Quantification by calculating the ratio of nuclear/cytoplasmic GFP signal intensity in each cell.

(C) Left and middle: Representative IHC staining of TERT in xenograft tumors from A549 cells without (control) or with TERC stably knocked down by its specific shRNA (TERC-sh) (400× magnification). Scale bar, 50 μm. Right: Quantification by calculating the percentage of the cells with nuclear staining of TERT. The numbers in the brackets in (B) and (C) denote the number of cells examined; and *p* values were determined by Student's *t*-test in comparison with the control.

trafficking of TERT. Another study showed that the association of TERT with TERC is a prerequisite for the localization of telomerase to telomeres in the nuclei of cancer cells.[49] Nonetheless, the subcellular location of telomerase assembly in human cells is still unclear.

Here, we demonstrated that the export of TERC into the cytoplasm was mediated by NXF1, a protein factor that mediates the nuclear export of lncRNAs and mRNAs with few exons,[36] but not the Ran GTPase-dependent karyopherin XPO1 (Figure 8A). Importantly, NXF1 knockdown not only blocked the nuclear export of TERC, but also caused a reduced amount of nuclear TERT (Figures 8C and 8D). These observations indicate that cytoplasmic TERC is essential for the assembly of the functional ribonucleoprotein complex, and only mature telomerase holoenzyme is imported into the nucleus. This assumption is supported by our results that TERC depletion hinders the interaction between TERT and another telomerase subunit SMG6, and the nuclear localization of this protein component (Figure 7). Accordingly, we propose a working model for the trafficking and assembly of telomerase in NSCLC cells (Figure 8F): (1) TERC is transcribed from its promoter by RNA polymerase II, and its 3′ end is processed. (2) The mature 451-nucleotide TERC is exported to the cytoplasm via the NXF1-mediated pathway. (3) TERT is translated in the cytoplasm and assembled into the catalytically active ribonucleoprotein complex with TERC, as well as other components of telomerase. (4) The properly assembled telomerase holoenzyme is imported into the nucleus, where it functions in telomere maintenance and transcriptional regulation.

Therapeutic potential of targeting TERC in NSCLC

Active telomerase requires the complexing of both TERT and TERC.[5] The small-molecule compound BIBR1532 binds to a conserved hydrophobic pocket on the surface of the C-terminal extension (CTE) domain of TERT, which is in close proximity to the telomerase RNA-binding domain (TRBD).[50] The CTE domain stabilizes the telomerase-telomeric DNA complex, while the TRBD interacts with TERC. Consequently, BIBR1532 interferes telomerase-mediated nucleotide addition on the one hand and destabilizes the telomerase ribonucleoprotein complex on the other. However, it remains unknown whether BIBR1532 also abolishes the non-canonical activities of telomerase.[51] In this study, our ChIP and RT-qPCR experiments showed that treatment of BIBR1532 did not influence the binding of TERT to its target genes or alter the RNA levels of these genes in A549 cells (Figures 5B and 5C). Also, BIBR1532 had no impact on the ROS in NSCLC cells (Figure S7C). These results imply that the BIBR1532-inhibited telomerase activity is dispensable to the non-canonical functions of TERT, which include gene expression regulation and mitochondrial protection.

Imetelstat is a lipid-conjugated oligonucleotide that competitively binds to the template region of TERC with high affinity and is the best-evaluated telomerase inhibitor.[13,51] So far, phase 2 clinical trials have been completed for imetelstat used alone in primary myelofibrosis, imetelstat + paclitaxel in treating metastatic breast cancer, and imetelstat + lenalidomide applied in multiple myeloma.[52] In regard to NSCLC, a phase 2 study demonstrated that imetelstat did not improve progression-free survival or overall survival in patients with long telomeres, and it failed to improve progression-free survival in patients with advanced NSCLC responding to first-line platinum-doublet chemotherapy.[14] This is probably that the efficacy of a telomerase-targeted therapy depends on the status of individual telomere length, for the onset of telomere dysfunction is determined by the shortest telomere in a cell.[53] Our current study in NSCLC has shown that depletion of TERC with its specific siRNAs impedes TERT nuclear localization and functions, causing telomere shortening and transcription repression of genes activated by TERT (Figures 5 and 6). Thus, targeting TERC by RNA interference-based therapeutics may be a feasible approach to NSCLC treatment.

Limitations of the study

Our current study has shown that hypomethylation of TERC promoter is associated with increased TERC level, which is correlated with disease progression and poor prognosis. Mechanistically, TERC facilitates the assembly and nuclear localization of the telomerase complex, thus enhancing the functions of TERT in telomere maintenance and transcription regulation. These observations provide insights into the functions of TERC in tumor growth and progression, suggesting that TERC is a potential target for NSCLC treatment. Nevertheless, it is worth mentioning that TERC is likely to have pro-survival functions in a telomerase-independent manner. Supporting evidence includes that TERC regulates DNA damage response pathways in cells that express no TERT,[54] and TERC has anti-apoptotic effects in human T cells independent of its function in telomerase activity.[28] TERC has also been reported to activate genes in the NF-κB and PI3K-AKT pathways through association with their promoters.[29,55] Our future research will investigate whether and how TERC promotes NSCLC cell survival and proliferation outside the telomerase complex.

STAR★METHODS

Detailed methods are provided in the online version of this paper and include the following:

- KEY RESOURCES TABLE
- RESOURCE AVAILABILITY
  - Lead contact

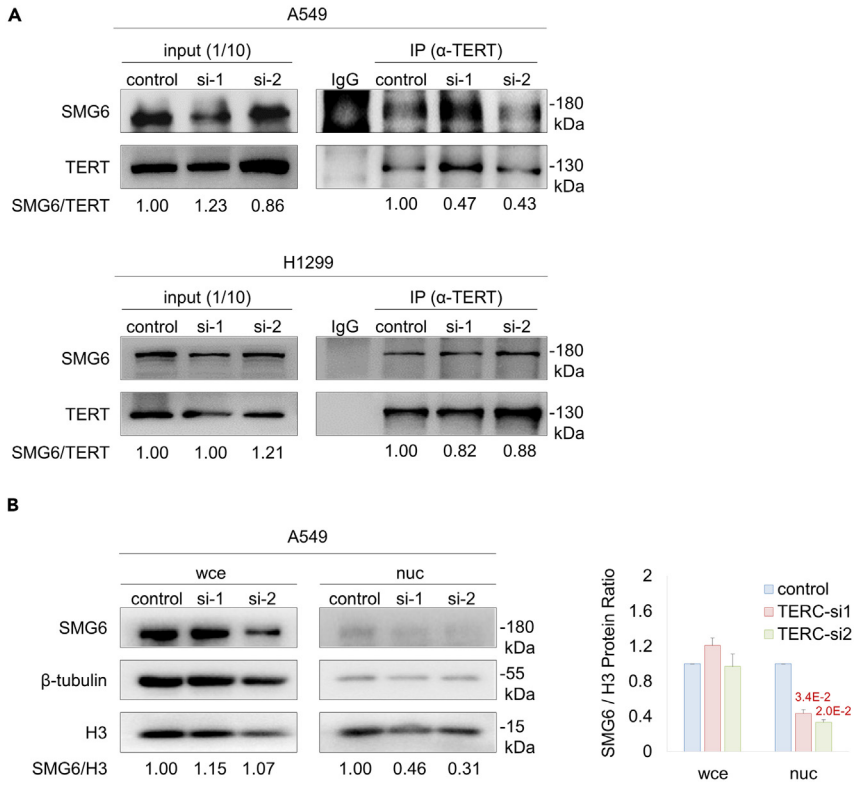

Figure 7. TERC mediates the assembly of the telomerase complex

(A) Interaction between TERT and SMG6 in NSCLC cells. TERT was immunoprecipitated with its specific antibody from control and TERC knockdown (si-1 and si-2) A549 and H1299 cells. IgG alone was used as a negative control. TERT and SMG6 were detected in the inputs and immunoprecipitates (IPs) by western blotting. The SMG6/TERT ratio of the control was set to 1.00, and the other ratios were measured relative to the control.

(B) Left: Representative images of western blotting to detect the level of SMG6 in whole-cell extracts (wce) and nuclear extracts (nuc) of A549 cells. β-tubulin served as whole cell and cytoplasmic loading control, while histone H3 served as whole cell and nuclear loading control. Numbers indicate the relative ratios of SMG6/histone H3. Right: Quantification of the blots. Data were presented as mean ± SD ($n \geq 2$), and p values were determined by Student's t-test in comparison with the control.

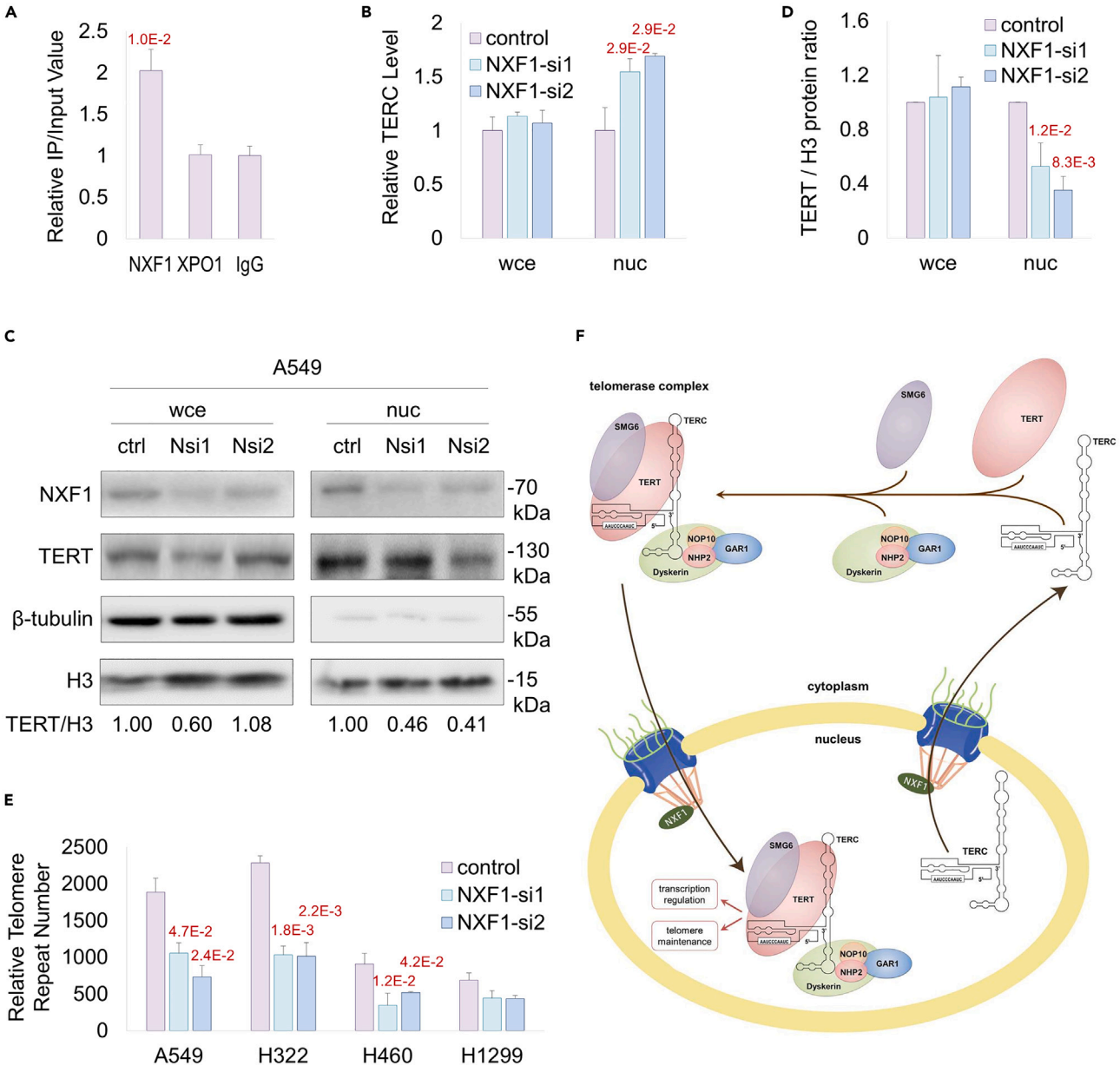

Figure 8. NXF1-exported TERC facilitates the cytoplasmic assembly of the telomerase complex and its subsequent nuclear localization

(A) Interaction between NXF1 and TERC. RIP assay was performed with NXF1 or XPO1 antibody on A549 cell lysates as previously described.[37] RIP with IgG served as control. RT-qPCR was performed to measure the amount of TERC in the precipitates. Data were presented as mean ± SD ($n \geq 3$), and p value was calculated by Student's t-test in comparison with the IgG control.

(B) Measurement of nuclear TERC enrichment by RT-qPCR. Whole-cell (wce) and nuclear (nuc) RNA extracts were prepared from A549 cells without (control) or with NXF1 knockdown (NXF1-si1, NXF1-si2). RT-qPCR was performed for each extract to measure the level of TERC, using U6 (known to remain in the nucleus after transcription by Pol III) as an internal control. Relative nuclear enrichment of TERC was determined by its nuclear/total expression normalized to the same ratio within the control. Data were presented as mean ± SD ($n \geq 2$), and p values were determined by Student's t-test in comparison with the control.

(C) Representative image of western blotting to detect TERT in A549 cells without (ctrl) or with NXF1 knocked down (Nsi1 and Nsi2). Numbers indicate the relative ratios of TERT/histone H3.

(D) Quantification of the blots in (C). Data were presented as mean ± SD ($n \geq 3$), and p values were analyzed by Student's t-test in comparison with the control.

(E) Relative telomere repeat number in NSCLC cells with NXF1 knockdown. Cellular DNA was extracted for qPCR to detect the telomere repeats, and 36B4 served as the single-copy gene control. Data are presented as mean ± SD (n ≥ 2). p values were determined by Student's t-test.

(F) A model for the trafficking and assembly of the telomerase components. The mature TERC is exported to the cytoplasm by NXF1, where it mediates the assembly of the telomerase ribonucleoprotein complex. The fully assembled telomerase holoenzyme is imported into the nucleus for telomere maintenance and transcriptional regulation.

- Measurement of mitochondrial membrane potential
- Immunohistochemistry (IHC)

- QUANTIFICATION AND STATISTICAL ANALYSIS

SUPPLEMENTAL INFORMATION

Supplemental information can be found online at https://doi.org/10.1016/j.isci.2024.109869.

ACKNOWLEDGMENTS

This work was supported by the National Natural Science Foundation of China (81972623 and 81702761 to M.C. and 82372650 and 82172949 to W.D.), Basic and Applied Basic Research Foundation of Guangdong Province (2020A1515010253 to M.C. and 2022A1515012508 to W.D.), and Shaoyang City Level Guiding Science and Technology Plan Project (2021073ZD to C.H.).

We thank Lanjun Zhang from the Department of Thorax at SYSUCC for help with the procurement of tumor samples. We thank Chi Kwan Tsang for constructive criticism and technical advice. We thank Lamei Huang, Changlin Zhang, Wei Liao, Lingyi Fu, Yixin Li, Kaping Lee, Fei Lin, and Zhen Wang for experimental assistance.

AUTHOR CONTRIBUTIONS

M.C. and W.D. designed research studies; H.S., X.L., Q.L., X.W., and W. Zhu performed the experiments and acquired data; H.S., X.L., Q.L., E.C., W. Zhou, C.H., and M.C. analyzed the data; H.Y. collected samples; H.S., W.D., and M.C. wrote the manuscript.

DECLARATION OF INTERESTS

The authors declare no competing interests.

Received: December 12, 2023
Revised: March 26, 2024
Accepted: April 29, 2024
Published: May 3, 2024

REFERENCES

1. Sung, H., Ferlay, J., Siegel, R.L., Laversanne, M., Soerjomataram, I., Jemal, A., and Bray, F. (2021). Global Cancer Statistics 2020: GLOBOCAN Estimates of Incidence and Mortality Worldwide for 36 Cancers in 185 Countries. CA A Cancer J. Clin. *71*, 209–249. https://doi.org/10.3322/caac.21660.
2. Hirsch, F.R., Scagliotti, G.V., Mulshine, J.L., Kwon, R., Curran, W.J., Jr., Wu, Y.-L., and Paz-Ares, L. (2017). Lung cancer: current therapies and new targeted treatments. Lancet *389*, 299–311. https://doi.org/10.1016/s0140-6736(16)30958-8.
3. Greider, C.W., and Blackburn, E.H. (1985). Identification of a specific telomere terminal transferase activity in Tetrahymena extracts. Cell *43*, 405–413. https://doi.org/10.1016/0092-8674(85)90170-9.
4. Cohen, S.B., Graham, M.E., Lovrecz, G.O., Bache, N., Robinson, P.J., and Reddel, R.R. (2007). Protein Composition of Catalytically Active Human Telomerase from Immortal Cells. Science *315*, 1850–1853. https://doi.org/10.1126/science.1138596.
5. Weinrich, S.L., Pruzan, R., Ma, L., Ouellette, M., Tesmer, V.M., Holt, S.E., Bodnar, A.G., Lichtsteiner, S., Kim, N.W., Trager, J.B., et al. (1997). Reconstitution of human telomerase with the template RNA component hTR and the catalytic protein subunit hTRT. Nat. Genet. *17*, 498–502. https://doi.org/10.1038/ng1297-498.
6. Jiang, J., Wang, Y., Sušac, L., Chan, H., Basu, R., Zhou, Z.H., and Feigon, J. (2018). Structure of Telomerase with Telomeric DNA. Cell *173*, 1179–1190.e13. https://doi.org/10.1016/j.cell.2018.04.038.
7. Cong, Y.-S., Wen, J., and Bacchetti, S. (1999). The Human Telomerase Catalytic Subunit hTERT: Organization of the Gene and Characterization of the Promoter. Hum. Mol. Genet. *8*, 137–142. https://doi.org/10.1093/hmg/8.1.137.
8. Yi, X., Tesmer, V.M., Savre-Train, I., Shay, J.W., and Wright, W.E. (1999). Both Transcriptional and Posttranscriptional Mechanisms Regulate Human Telomerase Template RNA Levels. Mol. Cell Biol. *19*, 3989–3997. https://doi.org/10.1128/mcb.19.6.3989.
9. Kim, N., Piatyszek, M., Prowse, K., Harley, C., West, M., Ho, P., Coviello, G., Wright, W., Weinrich, S., and Shay, J. (1994). Specific association of human telomerase activity with immortal cells and cancer. Science *266*, 2011–2015. https://doi.org/10.1126/science.7605428.
10. Hanahan, D., and Weinberg, R.A. (2011). Hallmarks of Cancer: The Next Generation. Cell *144*, 646–674. https://doi.org/10.1016/j.cell.2011.02.013.
11. Pestana, A., Vinagre, J., Sobrinho-Simões, M., and Soares, P. (2017). TERT biology and function in cancer: beyond immortalisation. J. Mol. Endocrinol. *58*, R129–R146. https://doi.org/10.1530/jme-16-0195.
12. Pascolo, E., Wenz, C., Lingner, J., Hauel, N., Priepke, H., Kauffmann, I., Garin-Chesa, P., Rettig, W.J., Damm, K., and Schnapp, A. (2002). Mechanism of Human Telomerase Inhibition by BIBR1532, a Synthetic, Non-nucleosidic Drug Candidate. J. Biol. Chem. *277*, 15566–15572. https://doi.org/10.1074/jbc.M201266200.
13. Guterres, A.N., and Villanueva, J. (2020). Targeting telomerase for cancer therapy. Oncogene *39*, 5811–5824. https://doi.org/10.1038/s41388-020-01405-w.
14. Chiappori, A.A., Kolevska, T., Spigel, D.R., Hager, S., Rarick, M., Gadgeel, S., Blais, N., Von Pawel, J., Hart, L., Reck, M., et al. (2015). A randomized phase II study of the telomerase inhibitor imetelstat as maintenance therapy for advanced non-small-cell lung cancer. Ann. Oncol. *26*, 354–362. https://doi.org/10.1093/annonc/mdu550.
15. Cong, Y., and Shay, J.W. (2008). Actions of human telomerase beyond telomeres. Cell Res. *18*, 725. https://doi.org/10.1038/cr.2008.74.
16. Martínez, P., and Blasco, M.A. (2011). Telomeric and extra-telomeric roles for telomerase and the telomere-binding proteins. Nat. Rev. Cancer *11*, 161. https://doi.org/10.1038/nrc3025.
17. Ding, D., Zhou, J., Wang, M., and Cong, Y.-S. (2013). Implications of telomere-independent activities of telomerase reverse transcriptase in human cancer. FEBS J. *280*, 3205–3211. https://doi.org/10.1111/febs.12258.
18. Park, J.-I., Venteicher, A.S., Hong, J.Y., Choi, J., Jun, S., Shkreli, M., Chang, W., Meng, Z., Cheung, P., Ji, H., et al. (2009). Telomerase modulates Wnt signalling by association with target gene chromatin. Nature *460*, 66. https://doi.org/10.1038/nature08137.
19. Liu, N., Ding, D., Hao, W., Yang, F., Wu, X., Wang, M., Xu, X., Ju, Z., Liu, J.-P., Song, Z., et al. (2016). hTERT promotes tumor angiogenesis by activating VEGF via interactions with the Sp1 transcription factor.

Nucleic Acids Res. *44*, 8693–8703. https://doi.org/10.1093/nar/gkw549.
20. Gonzalez, O.G., Assfalg, R., Koch, S., Schelling, A., Meena, J.K., Kraus, J., Lechel, A., Katz, S.-F., Benes, V., Scharffetter-Kochanek, K., et al. (2014). Telomerase stimulates ribosomal DNA transcription under hyperproliferative conditions. Nat. Commun. *5*, 4599. https://doi.org/10.1038/ncomms5599.
21. Khattar, E., Kumar, P., Liu, C.Y., Akıncılar, S.C., Raju, A., Lakshmanan, M., Maury, J.J.P., Qiang, Y., Li, S., Tan, E.Y., et al. (2016). Telomerase reverse transcriptase promotes cancer cell proliferation by augmenting tRNA expression. J. Clin. Investig. *126*, 4045–4060. https://doi.org/10.1172/jci86042.
22. Ahmed, S., Passos, J.F., Birket, M.J., Beckmann, T., Brings, S., Peters, H., Birch-Machin, M.A., von Zglinicki, T., and Saretzki, G. (2008). Telomerase does not counteract telomere shortening but protects mitochondrial function under oxidative stress. J. Cell Sci. *121*, 1046–1053. https://doi.org/10.1242/jcs.019372.
23. Haendeler, J., Dröse, S., Büchner, N., Jakob, S., Altschmied, J., Goy, C., Spyridopoulos, I., Zeiher, A.M., Brandt, U., and Dimmeler, S. (2009). Mitochondrial Telomerase Reverse Transcriptase Binds to and Protects Mitochondrial DNA and Function From Damage. Arterioscler. Thromb. Vasc. Biol. *29*, 929–935. https://doi.org/10.1161/ATVBAHA.109.185546.
24. Feng, J., Funk, W.D., Wang, S.-S., Weinrich, S.L., Avilion, A.A., Chiu, C.-P., Adams, R.R., Chang, E., Allsopp, R.C., Yu, J., et al. (1995). The RNA Component of Human Telomerase. Science *269*, 1236–1241. https://doi.org/10.1126/science.7544491.
25. Avilion, A.A., Piatyszek, M.A., Gupta, J., Shay, J.W., Bacchetti, S., and Greider, C.W. (1996). Human Telomerase RNA and Telomerase Activity in Immortal Cell Lines and Tumor Tissues. Cancer Res. *56*, 645–650.
26. Cayuela, M.L., Flores, J.M., and Blasco, M.A. (2005). The telomerase RNA component Terc is required for the tumour-promoting effects of Tert overexpression. EMBO Rep. *6*, 268–274. https://doi.org/10.1038/sj.embor.7400359.
27. Blasco, M.A., Rizen, M., Greider, C.W., and Hanahan, D. (1996). Differential regulation of telomerase activity and telomerase RNA during multi-stage tumorigenesis. Nat. Genet. *12*, 200–204. https://doi.org/10.1038/ng0296-200.
28. Gazzaniga, F.S., and Blackburn, E.H. (2014). An antiapoptotic role for telomerase RNA in human immune cells independent of telomere integrity or telomerase enzymatic activity. Blood *124*, 3675–3684. https://doi.org/10.1182/blood-2014-06-582254.
29. Wu, S., Ge, Y., Lin, K., Liu, Q., Zhou, H., Hu, Q., Zhao, Y., He, W., and Ju, Z. (2022). Telomerase RNA TERC and the PI3K-AKT pathway form a positive feedback loop to regulate cell proliferation independent of telomerase activity. Nucleic Acids Res. *50*, 3764–3776. https://doi.org/10.1093/nar/gkac179.
30. Yokoi, S., Yasui, K., Iizasa, T., Imoto, I., Fujisawa, T., and Inazawa, J. (2003). TERC Identified as a Probable Target within the 3q26 Amplicon That Is Detected Frequently in Non-Small Cell Lung Cancers. Clin. Cancer Res. *9*, 4705.
31. Selamat, S.A., Chung, B.S., Girard, L., Zhang, W., Zhang, Y., Campan, M., Siegmund, K.D., Koss, M.N., Hagen, J.A., Lam, W.L., et al. (2012). Genome-scale analysis of DNA methylation in lung adenocarcinoma and integration with mRNA expression. Genome Res. *22*, 1197–1211. https://doi.org/10.1101/gr.132662.111.
32. Li, L.-C., and Dahiya, R. (2002). MethPrimer: designing primers for methylation PCRs. Bioinformatics *18*, 1427–1431. https://doi.org/10.1093/bioinformatics/18.11.1427.
33. Cawthon, R.M. (2002). Telomere measurement by quantitative PCR. Nucleic Acids Res. *30*, e47. https://doi.org/10.1093/nar/30.10.e47.
34. Zheng, Q., Huang, J., and Wang, G. (2019). Mitochondria, Telomeres and Telomerase Subunits. Front. Cell Dev. Biol. *7*, 274. https://doi.org/10.3389/fcell.2019.00274.
35. Gallardo, F., Olivier, C., Dandjinou, A.T., Wellinger, R.J., and Chartrand, P. (2008). TLC1 RNA nucleo-cytoplasmic trafficking links telomerase biogenesis to its recruitment to telomeres. EMBO J. *27*, 748–757. https://doi.org/10.1038/emboj.2008.21.
36. Zuckerman, B., Ron, M., Mikl, M., Segal, E., and Ulitsky, I. (2020). Gene Architecture and Sequence Composition Underpin Selective Dependency of Nuclear Export of Long RNAs on NXF1 and the TREX Complex. Mol. Cell *79*, 251–267.e6. https://doi.org/10.1016/j.molcel.2020.05.013.
37. Chen, M., Long, Q., Borrie, M.S., Sun, H., Zhang, C., Yang, H., Shi, D., Gartenberg, M.R., and Deng, W. (2021). Nucleoporin TPR promotes tRNA nuclear export and protein synthesis in lung cancer cells. PLoS Genet. *17*, e1009899. https://doi.org/10.1371/journal.pgen.1009899.
38. Schmidt, J.C., and Cech, T.R. (2015). Human telomerase: biogenesis, trafficking, recruitment, and activation. Genes Dev. *29*, 1095–1105. https://doi.org/10.1101/gad.263863.115.
39. Wright, W.E., Piatyszek, M.A., Rainey, W.E., Byrd, W., and Shay, J.W. (1996). Telomerase activity in human germline and embryonic tissues and cells. Dev. Genet. *18*, 173–179. https://doi.org/10.1002/(sici)1520-6408(1996)18:2<173::Aid-dvg10>3.0.Co;2-3.
40. Bodnar, A.G., Ouellette, M., Frolkis, M., Holt, S.E., Chiu, C.P., Morin, G.B., Harley, C.B., Shay, J.W., Lichtsteiner, S., and Wright, W.E. (1998). Extension of life-span by introduction of telomerase into normal human cells. Science *279*, 349–352. https://doi.org/10.1126/science.279.5349.349.
41. Hahn, W.C., Stewart, S.A., Brooks, M.W., York, S.G., Eaton, E., Kurachi, A., Beijersbergen, R.L., Knoll, J.H., Meyerson, M., and Weinberg, R.A. (1999). Inhibition of telomerase limits the growth of human cancer cells. Nat. Med. *5*, 1164–1170. https://doi.org/10.1038/13495.
42. Zhang, X., Mar, V., Zhou, W., Harrington, L., and Robinson, M.O. (1999). Telomere shortening and apoptosis in telomerase-inhibited human tumor cells. Genes Dev. *13*, 2388–2399. https://doi.org/10.1101/gad.13.18.2388.
43. Cristofari, G., and Lingner, J. (2006). Telomere length homeostasis requires that telomerase levels are limiting. EMBO J. *25*, 565–574. https://doi.org/10.1038/sj.emboj.7600952.
44. Feng, J., Funk, W., Wang, S., Weinrich, S., Avilion, A., Chiu, C., Adams, R., Chang, E., Allsopp, R., Yu, J., et al. (1995). The RNA component of human telomerase. Science *269*, 1236–1241. https://doi.org/10.1126/science.7544491.
45. Soder, A.I., Hoare, S.F., Muir, S., Going, J.J., Parkinson, E.K., and Keith, W.N. (1997). Amplification, increased dosage and *in situ* expression of the telomerase RNA gene in human cancer. Oncogene *14*, 1013. https://doi.org/10.1038/sj.onc.1201066.
46. Andersson, S., Wallin, K.L., Hellström, A.C., Morrison, L.E., Hjerpe, A., Auer, G., Ried, T., Larsson, C., and Heselmeyer-Haddad, K. (2006). Frequent gain of the human telomerase gene TERC at 3q26 in cervical adenocarcinomas. Br. J. Cancer *95*, 331–338. https://doi.org/10.1038/sj.bjc.6603253.
47. Moore, L.D., Le, T., and Fan, G. (2013). DNA Methylation and Its Basic Function. Neuropsychopharmacology *38*, 23–38. https://doi.org/10.1038/npp.2012.112.
48. Chung, J., Khadka, P., and Chung, I.K. (2012). Nuclear import of hTERT requires a bipartite nuclear localization signal and Akt-mediated phosphorylation. J. Cell Sci. *125*, 2684–2697. https://doi.org/10.1242/jcs.099267.
49. Tomlinson, R.L., Abreu, E.B., Ziegler, T., Ly, H., Counter, C.M., Terns, R.M., and Terns, M.P. (2008). Telomerase Reverse Transcriptase Is Required for the Localization of Telomerase RNA to Cajal Bodies and Telomeres in Human Cancer Cells. Mol. Biol. Cell *19*, 3793–3800. https://doi.org/10.1091/mbc.e08-02-0184.
50. Bryan, C., Rice, C., Hoffman, H., Harkisheimer, M., Sweeney, M., and Skordalakes, E. (2015). Structural Basis of Telomerase Inhibition by the Highly Specific BIBR1532. Structure *23*, 1934–1942. https://doi.org/10.1016/j.str.2015.08.006.
51. Tomita, K., and Collopy, L.C. (2019). Telomeres, Telomerase, and Cancer. In Encyclopedia of Cancer, Third Edition, P. Boffetta and P. Hainaut, eds. (Academic Press), pp. 437–454. https://doi.org/10.1016/B978-0-12-801238-3.65017-1.
52. Vishwakarma, K., Dey, R., and Bhatt, H. (2023). Telomerase: A prominent oncological target for development of chemotherapeutic agents. Eur. J. Med. Chem. *249*, 115121. https://doi.org/10.1016/j.ejmech.2023.115121.
53. Hemann, M.T., Strong, M.A., Hao, L.Y., and Greider, C.W. (2001). The shortest telomere, not average telomere length, is critical for cell viability and chromosome stability. Cell *107*, 67–77. https://doi.org/10.1016/s0092-8674(01)00504-9.
54. Kedde, M., le Sage, C., Duursma, A., Zlotorynski, E., van Leeuwen, B., Nijkamp, W., Beijersbergen, R., and Agami, R. (2006). Telomerase-independent regulation of ATR by human telomerase RNA. J. Biol. Chem. *281*, 40503–40514. https://doi.org/10.1074/jbc.M607676200.
55. Liu, H., Yang, Y., Ge, Y., Liu, J., and Zhao, Y. (2019). TERC promotes cellular inflammatory response independent of telomerase. Nucleic Acids Res. *47*, 8084–8095. https://doi.org/10.1093/nar/gkz584.

STAR★METHODS

KEY RESOURCES TABLE

REAGENT or RESOURCE	SOURCE	IDENTIFIER
Antibodies		
Rabbit monoclonal [Y182] anti-TERT	Abcam	Cat#ab32020; RRID: AB_778296
Rabbit polyclonal anti-SMG6	Abcam	Cat#ab87539; RRID: AB_10674461
Rabbit polyclonal unconjugated antibody	Cell Signaling Technology	Cat#2729; RRID: AB_1031062
Rabbit monoclonal (92G2) anti-Cyclin D1	Cell Signaling Technology	Cat#2978; RRID: AB_2259616
Rabbit monoclonal (D6V7N) anti-exportin-1/CRM1	Cell Signaling Technology	Cat#46249; RRID: AB_2799298
Rabbit polyclonal anti-NXF1	Proteintech	Cat#10328-1-AP; RRID: AB_2236500
Mouse monoclonal anti-β-tubulin	Proteintech	Cat#66240-1-Ig; RRID: AB_2881629
Rabbit polyclonal anti-Histone-H3	Proteintech	Cat#17168-1-AP; RRID: AB_2716755
HRP-conjugated Affinipure Goat anti-Mouse IgG(H+L)	Proteintech	Cat#SA00001-1; RRID: AB_2722565
HRP-conjugated Affinipure Goat anti-Rabbit IgG(H+L)	Proteintech	Cat#SA00001-2; RRID: AB_2722564
FITC-conjugated Goat anti-Rabbit IgG (H+L)	ABclonal	Cat#AS011; RRID: AB_2769476
Bacterial and virus strains		
E. coli Stbl3	Thermo Fisher Scientific-Invitrogen	Cat#C737303
Biological samples		
NSCLC tissues	SYSUCC Tumor Bio-bank	https://english.sysucc.org.cn/index_31.aspx See Table S1 for sample information
Chemicals, peptides, and recombinant proteins		
BIBR1532	Selleck Chemicals	Cat#S1186; CAS: 321674-73-1
5-Azacytidine	MedChemExpress	Cat#HY-10586; CAS: 320-67-2
RPMI-1640 Medium	Thermo Fisher Scientific-Gibco	Cat#11875093
Dulbecco's Modified Eagle Medium	Thermo Fisher Scientific-Gibco	Cat#10564011
Dynabeads Protein G for Immunoprecipitation	Thermo Fisher Scientific-Invitrogen	Cat#10003D
Lipofectamine 3000 Transfection Reagent	Thermo Fisher Scientific-Invitrogen	Cat#L3000015
Polybrene	Santa Cruz Biotechnology	Cat#sc-134220; CAS: 28728-55-4
Corning Matrigel Basement Membrane Matrix	Corning	Cat#356234
Critical commercial assays		
DNA/RNA co-Extraction Kit	TIANGEN	Cat#DP422
Universal Genomic DNA Purification Mini Spin Kit	Beyotime	Cat#D0063
BeyoFast SYBR Green qPCR Mix (2X)	Beyotime	Cat#D7260
RNAeasy Animal Total RNA Isolation Kit with Spin Column	Beyotime	Cat#R0032
BeyoRTII First Strand cDNA Synthesis Kit (RNase H minus)	Beyotime	Cat#D7168
BeyoFast SYBR Green qPCR Mix (2×)	Beyotime	Cat#D7260
Reactive Oxygen Species Assay Kit	Beyotime	Cat#S0033
TMRE-Mitochondrial Membrane Potential Assay Kit	Abcam	Cat#ab113852
PI/RNase Staining Buffer	BD Biosciences	Cat#550825
DNA Bisulfite Conversion Kit	Beyotime	Cat#D0068

(*Continued on next page*)

Continued

REAGENT or RESOURCE	SOURCE	IDENTIFIER
Deposited data		
GSE32863	Selamat et al.[31]	https://www.ncbi.nlm.nih.gov/geo/
TCGA Lung Adenocarcinoma (LUAD)	UCSC Xena	http://xena.ucsc.edu/
TCGA Lung Squamous Cell Carcinoma (LUSC)	UCSC Xena	http://xena.ucsc.edu/
Experimental models: Cell lines		
Human: A549	ATCC	Cat#CCL-185; RRID: CVCL_0023
Human: H322	Sigma Aldrich	Cat#95111734; RRID: CVCL_1556
Human: H460	ATCC	Cat#HTB-177; RRID: CVCL_0459
Human: H1299	ATCC	Cat#CRL-5803; RRID: CVCL_0060
Human: HEK293T	ATCC	Cat#CRL-3216; RRID: CVCL_0063
Mouse: LL/2 (LLC1)	ATCC	Cat#CRL-1642; RRID: CVCL_4358
Experimental models: Organisms/strains		
Mouse: BALB/c female nude mice	Guangdong Medical Laboratory Animal Center	RRID: IMSR_JAX:002019
Mouse: C57BL/6J female mice	Guangdong Medical Laboratory Animal Center	RRID: IMSR_JAX:000664
Oligonucleotides		
Primers for gene knockdown	This study	See Table S2
Primers for telomere repeat number measurement	Cawthon[33]	See Table S2
Primers for methylation specific PCR	This study	See Table S2
Primers for RT-qPCR	This study	See Table S2
Primers for ChIP-qPCR	This study	See Table S2
Recombinant DNA		
pLKO.1 puro	addgene	Cat#8453; RRID: Addgene_8453
psPAX2	addgene	Cat#12260; RRID: Addgene_12260
pMD2.G	addgene	Cat#12259; RRID: Addgene_12259
Software and algorithms		
Fiji ImageJ	National Institutes of Health	N/A
ModFit LT	Verity Software House	Version#4.1
MethPrimer	Li and Dahiya[32]	https://www.urogene.org/methprimer/
GraphPad Prism	GraphPad Software	Version#8.3.0

RESOURCE AVAILABILITY

Lead contact

Further information and requests for resources and reagents should be directed to and will be fulfilled by the Lead Contact, Miao Chen (chenmiao@sysucc.org.cn).

Materials availability

This study did not generate new unique reagents.

Data and code availability

- All data reported in this paper will be shared by the lead contact upon request. Gene methylation data (β values) and RNA expression data of the TCGA cohort were downloaded from UCSC Xena (https://xena.ucsc.edu/). RNA expression data of the GSE32863 series were from Gene Expression Omnibus (https://www.ncbi.nlm.nih.gov/geo/).
- This paper does not report original code.
- Any additional information required to reanalyze the data reported in this paper is available from the lead contact upon request.

EXPERIMENTAL MODEL AND STUDY PARTICIPANT DETAILS

Cell lines

A549, H460, H1299, HEK-293T and LLC cells were obtained from the American Type Culture Collection (ATCC). H322 cells were purchased from Sigma Aldrich. A549, H322, H460 and H1299 cells were cultured in RPMI-1640 medium supplemented with 10% fetal bovine serum (FBS), while HEK-293T and LLC cells were cultured in Dulbecco's modified Eagle's medium (DMEM) supplemented with 10% FBS. All cells were maintained at 37°C in a humidified incubator with 5% CO_2.

Tissue samples

This study had been reviewed and approved by the Institutional Review Board of Sun Yat-sen University Cancer Center (SYSUCC, No. GZR2019-077). All the experiments conformed to the principles set out in the WMA Declaration of Helsinki and the Department of Health and Human services Belmont Report. 20 pairs of NSCLC and adjacent normal tissue samples, as well as another 354 NSCLC tissue samples were collected from patients who had surgery from January 2009 to December 2015 at SYSUCC. Demographic and clinicopathological parameters of the patients are listed in Table S1. Tissue DNA and RNA samples were prepared using DNA / RNA co-Extraction Kit (TIANGEN DP422).

Mice

Animal experiment protocols had been approved by the Institutional Animal Care and Use Committee of Sun Yat-sen University Cancer Center (No. L102012019005N). Female BALB/c athymic nude mice aged 4 weeks were subcutaneously injected in the flank with 1×10^7 A549 cells without (control) or with TERC stably knocked down (TERC-sh) in 0.1 mL Matrigel (Corning 356234). Female C57BL/6 mice aged 4 weeks were subcutaneously injected in the flank with 3×10^6 LLC cells without (control) or with mouse TERC stably knocked down (TERC-sh). Xenograft tumor formation was monitored by length and width measurement with a caliper, and tumor size was calculated by the formula: size = $\pi/6 \times$ length $\times$ width^2. At the end of the experiment, the mice were sacrificed and the xenograft tumors were collected, photographed and fixed in 4% paraformaldehyde.

METHOD DETAILS

DNA modification by sodium bisulfite and amplification by methylation-specific PCR (MSP)

Cellular genomic DNA was isolated with the Universal Genomic DNA Purification Mini Spin Kit (Beyotime). Bisulfite modification of DNA was performed with the DNA Bisulfite Conversion Kit (Beyotime) per the manufacturer's directions. Bisulfite-treated DNA was amplified by PCR. The primers used were designed by MethPrimer (https://www.urogene.org/methprimer/, Li and Dahiya[32]), and their sequences were described in Table S2.

RNAi and transfection

siRNA sequences are listed in Table S2. siRNA transfection was performed with Lipofectamine 3000 Transfection Reagent (Thermo Fisher Scientific-Invitrogen) according to the manufacturer's instruction.

The knockdown plasmids were derived from pLKO.1 (addgene). pLKO.1 was cut open with *Age*I and *Eco*RI, re-ligated with annealed oligos containing short hairpin sequences to knock down TERC (Table S2), transformed into Stbl3 competent cells and confirmed by sequencing.

To establish TERC knockdown (TERC-sh) and control stable cells, pLKO.1-TERC-sh or pLKO.1 together with psPAX2 (addgene) and pMD2.G (addgene) plasmids were co-transfected into HEK-293T cells. The virus-containing media were harvested 48 hours after transfection, filtered with a 0.22 μm unit, and added to A549 cells that were approximately 70% confluent and cultured in fresh media with 8 μg/mL Polybrene (Santa Cruz). 24 hours after infection, media were changed and 2 μg/mL puromycin was added to select for positive clones for at least one week.

Telomere length measurement

DNA was isolated using the Universal Genomic DNA Purification Mini Spin Kit (Beyotime). Telomere length was measured by the quantitative PCR (qPCR) method described by Cawthon.[33] qPCR was performed on the Roche LightCycler 480 System using the BeyoFast SYBR Green qPCR Mix (2×), with the "tel 1" and "tel 2" primer pair to amplify the telomere repeats (T), and the "36B4u" and "36B4d" primer pair to amplify the single copy gene (S) that serves as the internal reference. The primer sequences were listed in Table S2. The thermal cycling profile for both amplicons began with a 95°C incubation for 1 minute for initial denaturation, followed by 40 cycles of 95°C for 10 seconds, 54°C for 15 seconds, and 72°C for 2 minutes. The relative telomere length was determined by the T/S ratio by the $2^{-\Delta\Delta CT}$ method.

Separation of nuclear and cytoplasmic fractions

Nuclear and cytoplasmic fraction separation was performed per the Nuclear Extraction Protocol provided on the Thermo Fisher Scientific website (https://www.thermofisher.com/hk/en/home/references/protocols.html/). In brief, 5×10^6 cells were washed twice with ice-cold PBS, collected, resuspended in 500 μL hypotonic buffer (20 mM Tris-HCl pH 7.4, 10 mM NaCl, 3 mM $MgCl_2$) by pipetting several times,

and incubated on ice for 15 minutes. 25 μL 10% NP-40 was then added, and the homogenate was vortexed for 10 seconds at highest setting before centrifugation at 3,000 rpm at 4°C. The supernatant contained the cytoplasmic fraction, while the pellet was the nuclear fraction.

RNA extraction and RT-qPCR

RNA was extracted using the RNAeasy Animal Total RNA Isolation Kit with Spin Column (Beyotime). Reverse transcription (RT) was performed with the BeyoRTII First Strand cDNA Synthesis Kit (RNase H minus) (Beyotime) with gene-specific primers, followed by qPCR with the primers listed in Table S2. The relative RNA level was determined by the $2^{-\Delta\Delta CT}$ method.

Protein extraction and western blotting

Cells were lysed at 4°C with RIPA buffer (1% Triton X-100, 1% deoxycholate and 0.1% SDS, Beyotime P0013B) containing protease and phosphatase inhibitors and PMSF, and centrifuged at 12,000 ×g for 15 minutes to collect the supernatant. Protein lysates were separated by SDS-polyacrylamide gel electrophoresis (PAGE) and transferred to 0.2 μm PVDF membranes (Roche 03010040001). The membrane was blocked with 5% nonfat milk in PBST for 1 hour at room temperature, incubated with primary antibodies overnight at 4°C, washed three times with PBST, incubated with secondary antibodies for 30 minutes at room temperature, washed three more times with PBST, developed using the enhanced chemiluminescent (ECL) detection reagents, visualized with ChemiDoc Touch Imaging System (Bio-Rad), and quantified with Image J software.

Co-immunoprecipitation (co-IP)

Cells were lysed with RIPA buffer (1% NP-40 and 0.25% deoxycholate, Beyotime P0013D) containing protease and phosphatase inhibitors and PMSF, and centrifuged at 12,000 ×*g* for 15 minutes to collect the supernatant. 2,000 μg total protein in 0.5 mL was incubated with anti-TERT (Abcam) antibody overnight at 4°C with rotation. A sample incubated with IgG was included as control. Dynabeads protein G (Thermo Fisher Scientific-Invitrogen) were added to the antibody conjugated complex and incubated for 2 hours at 4°C with rotation. Afterward, the beads were washed three times with washing buffer A (50 mM Tris-HCl, pH 7.5, 0.5% Triton X-100, 150 mM NaCl, 2 mM $CaCl_2$, 5% glycerol, 2 mM PMSF), once with washing buffer B (50 mM Tris-HCl, pH 7.5, 0.5% Triton X-100, 500 mM NaCl, 2 mM $CaCl_2$, 5% glycerol, 2 mM PMSF), and twice with washing buffer C (50mM Tris-HCl, pH 7.5, 150 mM NaCl, 2 mM $CaCl_2$). The bound materials were eluted by boiling in SDS protein sample buffer, and analyzed by western blotting.

RNA immunoprecipitation (RIP)

RIP was performed as described by Chen et al.[37] Cells were first fixed, lysed, sonicated and centrifuged. Then, the supernatant was collected and incubated with anti-NXF1 (Proteintech) or anti-XPO1 (Cell Signaling Technology) antibody overnight at 4°C with rotation. A sample incubated with IgG was included as control. The next morning, Dynabeads protein G were added to the antibody conjugated complex and incubated for 2 hours at 4°C with rotation. Afterward, the beads were washed and incubated for 1 hour at 70°C to reverse cross-link. Immunoprecipitated RNA was extracted with RNAeasy Animal Total RNA Isolation Kit (Beyotime), and analyzed by RT-qPCR with the primers listed in Table S2.

Chromatin immunoprecipitation (ChIP)

ChIP was performed based on the X-ChIP protocol by abcam (https://www.abcam.com/protocols/). Anti-TERT antibody (Abcam) was used for immunoprecipitation, and IgG was used for control. Dynabeads protein G were used to recover the antibody-antigen-DNA complexes. The primers for qPCR detection were listed in Table S2.

Immunofluorescence (IF)

Cells were grown in glass bottom culture dish (NEST Scientific 801002), fixed with 4% paraformaldehyde at room temperature for 30 minutes, and washed three times with PBS. Afterward, cells were permeabilized with 0.25% Triton X-100 in PBS at room temperature for 30 minutes, washed three times with PBS, blocked with 5% bovine serum albumin (BSA) in PBS at room temperature for 45 minutes, and incubated with anti-TERT antibody (Abcam, 1:500 dilution) in a humid chamber overnight at 4°C. The next day, cells were washed three times with PBS, followed by detection with FITC-conjugated secondary antibodies (ABclonal, 1:500 dilution). DNA was stained with 10 μg/mL 4′,6-diamidino-2-phenylindole (DAPI) for 10 minutes. Images were acquired using a Zeiss LSM 880 with Airyscan confocal laser scanning microscope (60× objective). In the FITC channel, circular regions of 80 pixels were randomly selected in the nucleus and the cytoplasm. The mean grey value (MGV) for each region was measured, and the ratio of nuclear/cytoplasmic TERT distribution was determined as MGVnucleus / MGVcytoplasm.

Colony formation

Cells were seeded in six-well plates (800 cells / well) and allowed to grow for 7 days. Subsequently, colonies formed were fixed with 4% paraformaldehyde for 10 minutes at room temperature, washed twice with H_2O, stained with crystal violet for 5 minutes, washed again with H_2O for three times to remove excessive dye, and counted after air-dry overnight.

Transwell migration assay

2×10^4 cells were seeded in each upper chamber of Transwell plates (Corning 3401). RPMI-1640 medium supplemented with 10% FBS was added to the bottom chamber. After 24 hours of incubation at 37°C, cells that remained in the upper chamber were removed with a cotton swab. Cells that had migrated through the membrane were fixed with methanol, stained with 0.1% crystal violet, and washed with H_2O to remove excessive dye, before getting imaged by microscope.

Cell cycle analysis

Cells were harvested and fixed in pre-chilled 70% ethanol at 4°C overnight. The next day, cells were washed twice with PBS, and incubated in PI/RNase staining buffer (BD Biosciences) at room temperature for 15 minutes. Afterward, cell numbers in different cell cycle stages were counted by CytoFLEX benchtop flow cytometer (Beckman Coulter), and the data were analyzed by ModFit LT 4.1 software.

Reactive oxygen species (ROS) detection

ROS was detected with Reactive Oxygen Species Assay Kit (Beyotime), which uses the cell permeant reagent 2',7'-dichlorofluorescin diacetate (DCFDA, also known as H2DCFDA, DCFH-DA, and DCFH) to quantitatively assess ROS in live cell samples. Cells were collected, stained with DCFDA for 20 minutes at 37°C in the dark, and analyzed by flow cytometer with excitation / emission at 488 nm / 525 nm.

Measurement of mitochondrial membrane potential

Mitochondrial membrane potential was measured using TMRE-Mitochondrial Membrane Potential Assay Kit (Abcam). Cells were incubated with tetramethylrhodamine ethyl ester (TMRE) for 15-30 minutes to label active mitochondria, washed with PBS containing 0.2% BSA, and analyzed by flow cytometer with excitation / emission at 488 nm / 575 nm. For control cells, carbonyl cyanide 4-(trifluoromethoxy) phenylhydrazone (FCCP), an ionophore uncoupler of oxidative phosphorylation, was added for 10 minutes before TMRE treatment, so as to eliminate mitochondrial membrane potential and TMRE staining.

Immunohistochemistry (IHC)

4 μm tissue sections were prepared from paraffin-embedded xenograft tumors. For IHC analysis, the sections were deparaffinized, and subjected to antigen retrieval and blocking. Subsequently, primary antibodies were diluted 1:100 and added in for incubation at 4°C overnight in a humidified chamber. The next day, chromogen-based detection was performed with LSAB+, Dako REAL Detection Systems (Agilent K500511-2).

The IHC scores were determined by the staining intensity and the percentage of positive cells. The staining intensity was graded as "0" for no brown particle staining, "1" for light brown staining, "2" for moderate brown staining, and "3" for dark brown staining. The percentage of positive cells was converted to "0" for <10% positive cells, "1" for 10-40% positive cells, "2" for 40-70% positive cells, and "3" for ≥70% positive cells. These two scores were multiplied to generate the IHC score. For subcellular localization analysis, cells with 3 or more brown punctate spots in their nuclei were considered to have nuclear staining.

QUANTIFICATION AND STATISTICAL ANALYSIS

All of the statistical details of experiments can be found in the figure legends. Statistical analysis was performed using GraphPad Prism 8.3.0.